Article

Cell

LECT2, a Ligand for Tie1, Plays a Crucial Role in Liver Fibrogenesis

Graphical Abstract

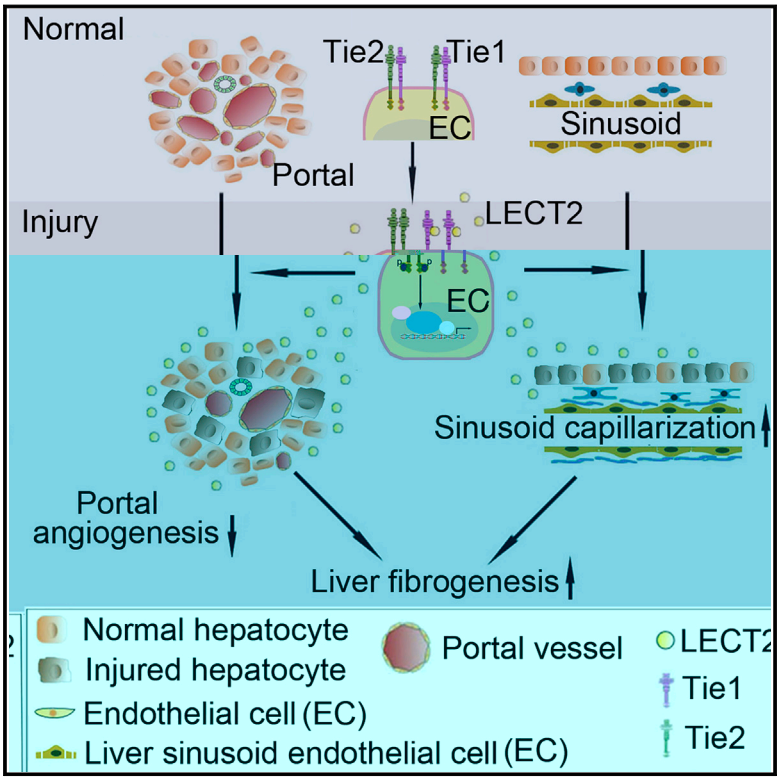

Highlights

- LECT2 is a functional ligand of EC-specific orphan receptor Tie1
- LECT2-Tie1 inhibits portal angiogenesis and promotes sinusoid capillarization
- LECT2-Tie1 promotes liver fibrogenesis
- Divergent roles of portal angiogenesis and sinusoid capillarization in liver fibrosis

Authors

Meng Xu, Hong-Hai Xu, Yuan Lin, ..., Dalei Wu, Yan-Qing Ding, Wei-Jie Zhou

Correspondence

dyqgz@126.com (Y.-Q.D.), weijiezhouum@163.com (W.-J.Z.)

In Brief

Produced by hepatocytes in response to liver damage, LECT2 signals through orphan receptor Tie1 on endothelial cells to activate Tie2 signaling in endothelial cells and promote fibrosis.

Xu et al., 2019, Cell *178*, 1–15
September 5, 2019
https://doi.org/10.1016/j.cell.2019.07.021

CellPress

Please cite this article in press as: Xu et al., LECT2, a Ligand for Tie1, Plays a Crucial Role in Liver Fibrogenesis, Cell (2019), https://doi.org/10.1016/j.cell.2019.07.021

Article

Cell

LECT2, a Ligand for Tie1, Plays a Crucial Role in Liver Fibrogenesis

Meng Xu,[1,2,3,16] Hong-Hai Xu,[1,2,3,4,16] Yuan Lin,[1,2,3,5,16] Xiangnan Sun,[6] Li-Jing Wang,[7] Zhe-Ping Fang,[8] Xue-Han Su,[1,2,3] Xiang-Jing Liang,[1,2,3] Yang Hu,[1,2,3] Zhi-Min Liu,[1,2,3] Yuanxiong Cheng,[9] Yuanyuan Wei,[4] Jiabin Li,[4] Li Li,[7] Hong-Juan Liu,[10] Zhiqiang Cheng,[11] Na Tang,[11] Chao Peng,[12] Tingting Li,[1,2,3] Tengfei Liu,[1,2,3] Liang Qiao,[13] Dalei Wu,[6] Yan-Qing Ding,[1,2,3,*] and Wei-Jie Zhou[1,2,3,5,14,15,17,*]

[1]Department of Pathology, Nanfang Hospital, Southern Medical University, Guangzhou, Guangdong 510515, China
[2]Department of Pathology, School of Basic Medical Sciences, Southern Medical University, Guangzhou, Guangdong 510515, China
[3]Guangdong Province Key Laboratory of Molecular Tumor Pathology, Guangzhou, Guangdong 510515, China
[4]The First Affiliated Hospital of Anhui Medical University, Anhui, Hefei 230022, China
[5]Shunde Hospital, Southern Medical University (The First People's Hospital of Shunde Foshan), Shunde, Guangdong 528333, China
[6]Helmholtz International Lab, State Key Laboratory of Microbial Technology, Shandong University, Qingdao, Shandong 266237, China
[7]Vascular Biology Research Institute, School of Life Sciences and Biopharmaceuticals, Guangdong Pharmaceutical University, Guangzhou, Guangdong 510006, China
[8]Department of Hepatobiliary Surgery, Taizhou Hospital of Zhejiang Province, Wenzhou Medical University, Linhai, Zhejiang 317000, China
[9]Department of Respiratory and Critical Care Medicine, The Third Affiliated Hospital, Southern Medical University, Guangzhou, Guangdong 510630, China
[10]Department of Bioinformation, School of Basic Medical Sciences, Southern Medical University, Guangzhou, Guangdong 510515, China
[11]Department of Pathology, Shenzhen People's Hospital, Shenzhen, Guangdong 515020, China
[12]National Facility for Protein Science in Shanghai, Zhangjiang Lab, Shanghai 201210, China
[13]Storr Liver Centre, Westmead Institute for Medical Research, The University of Sydney and Westmead Hospital and Western Clinical School, Westmead, NSW 2145, Australia
[14]Microbiome Medicine Center, Zhujiang Hospital, Southern Medical University, Guangzhou, Guangdong 510515, China
[15]Guangzhou Regenerative Medicine and Health Guangdong Laboratory, Guangzhou, Guangdong 510005, China
[16]These authors contributed equally
[17]Lead Contact
*Correspondence: dyqgz@126.com (Y.-Q.D.), weijiezhouum@163.com (W.-J.Z.)
https://doi.org/10.1016/j.cell.2019.07.021

SUMMARY

Liver fibrosis is a very common condition seen in millions of patients with various liver diseases, and yet no effective treatments are available owing to poorly characterized molecular pathogenesis. Here, we show that leukocyte cell-derived chemotaxin 2 (LECT2) is a functional ligand of Tie1, a poorly characterized endothelial cell (EC)-specific orphan receptor. Upon binding to Tie1, LECT2 interrupts Tie1/Tie2 heterodimerization, facilitates Tie2/Tie2 homodimerization, activates PPAR signaling, and inhibits the migration and tube formations of EC. *In vivo* studies showed that LECT2 overexpression inhibits portal angiogenesis, promotes sinusoid capillarization, and worsens fibrosis, whereas these changes were reversed in *Lect2-KO* mice. Adeno-associated viral vector serotype 9 (AAV9)-LECT2 small hairpin RNA (shRNA) treatment significantly attenuates fibrosis. Upregulation of LECT2 is associated with advanced human liver fibrosis staging. We concluded that targeting LECT2/Tie1 signaling may represent a potential therapeutic target for liver fibrosis, and serum LECT2 level may be a potential biomarker for the screening and diagnosis of liver fibrosis.

INTRODUCTION

Liver fibrosis is a condition with excessive deposition of extracellular matrixes such as collagens and fibronectin in the liver tissue as a result of repeated liver injury often seen in patients with chronic liver diseases (CLDs). The most common causative conditions for liver fibrosis include chronic viral hepatitis, alcoholic liver disease, non-alcoholic steatohepatitis (NASH), and autoimmune hepatitis (Gressner and Weiskirchen, 2006; Tsochatzis et al., 2014). Without effective intervention, liver fibrosis leads to liver cirrhosis, one of the most common causes of death worldwide (Lim and Kim, 2008).

The tyrosine kinase with immune globulin-like and epidermal growth factor homology (Tie) family of receptor tyrosine kinases, comprising Tie1 and Tie2, was first reported in 1992 (Partanen et al., 1992). Previous studies have revealed that both Tie1 and Tie2, as well as their interactions, play important roles in the pathogenesis of human diseases through regulating angiogenesis (Augustin et al., 2009). Tie1, per se, is largely an orphan receptor for angiogenesis, but it has been shown to bind to and regulate the activity of Tie2 and thus plays an essential role in the development and function of normal vasculature (Kim et al., 2006; Saharinen et al., 2005; Seegar et al., 2010; Savant et al., 2015). Tie1 deficiency results in mid- to late-gestation embryonic lethality due to impaired vasculature development as manifested by severe edema, hemorrhage, and loss of microvascular integrity (Puri et al., 1995; Qu et al., 2010; Sato et al., 1995).

Please cite this article in press as: Xu et al., LECT2, a Ligand for Tie1, Plays a Crucial Role in Liver Fibrogenesis, Cell (2019), https://doi.org/10.1016/j.cell.2019.07.021

Leukocyte cell-derived chemotaxin 2 (LECT2) is a 16-kDa secreted protein (Ito et al., 2003) originally identified as a chemotactic factor for neutrophils that can stimulate the growth of chondrocytes and osteoblasts (Yamagoe et al., 1996). Recently, accumulated evidence indicates that LECT2 is involved in many pathological conditions, such as sepsis (Lu et al., 2013), diabetes (Lan et al., 2014), systemic amyloidosis (Mereuta et al., 2014), hepatocarcinogenesis (Ong et al., 2011), non-alcoholic fatty liver disease (NAFLD) (Yoo et al., 2017), and expansion/mobilization of hematopoietic stem cells (Lu et al., 2016). However, the role of LECT2 in the development of liver fibrosis and the underlying mechanisms remain largely unclear.

This study reports our novel findings on the important role of LECT2/Tie1 signaling in pathogenesis of liver fibrosis and the underlying mechanisms. The serum LECT2 level may represent a potential diagnostic marker for liver fibrosis, and more importantly, LECT2 may serve as a potential therapeutic target for liver fibrosis.

RESULTS

Expression Level of LECT2 Correlated with Liver Fibrosis Staging

We first detected the expression of LECT2 in human normal and fibrotic liver samples using immunohistochemical analysis. In the normal livers, low level of LECT2 was seen in hepatocytes surrounding central veins, whereas in the fibrotic livers, significantly stronger LECT2 expression was observed in the areas surrounding portal vessels and damage boundaries (Figure 1A; Table S1). Fibrotic liver samples showed much higher mRNA levels of LECT2 than the normal livers (Figure 1B). Patients with liver fibrosis showed significantly higher levels of serum LECT2 as compared to the healthy controls (Figure 1C; Table S2). Notably, the extent of serum LECT2 elevation was more significant (by ~6-fold) than that of the alanine aminotransferase (ALT) (by ~3-fold) (Figure 1D). By using Spearman correlation analysis, we observed a significant correlation between the serum ALT and LECT2 levels in 152 patients ($r = 0.2681$, $p < 0.0008$, Figure 1E).

We next evaluated if the serum level of LECT2 could be used as a diagnostic biomarker for liver fibrosis regardless of the etiologies. The cohort of 152 patients included hepatitis B-related cirrhosis, cryptogenic cirrhosis, alcoholic cirrhosis, hepatitis B plus alcoholic cirrhosis, autoimmune hepatitis-related cirrhosis ($n = 6$), primary biliary cirrhosis, hepatitis C-related cirrhosis, and hepatitis C plus schistosomiasis-related cirrhosis. Significant increase in the serum LECT2 levels was seen in all these patients as compared to the normal subjects (Figure 1F).

Increased serum ALT levels can be clearly observed when the liver is undergoing damage, but is seldom observed when the liver enters the stable cirrhosis stage. We next asked whether increased serum LECT2 levels could be observed in patients with normal serum ALT levels. The serum samples of the cirrhotic liver patients were divided into two groups based on their serum ALT levels: normal and abnormal. Interestingly, the patients with normal serum ALT showed significant elevations in the serum LECT2 levels (Figures 1G and 1H). By immunohistochemical staining, we found a significantly higher level of LECT2 expression in the liver tissues together with more abundant $LECT2^+$ cells in high-grade liver cirrhosis than in low-grade liver cirrhosis (based on Child-Pugh classification) (Figures 1I and 1J). Unlike the serum ALT levels and AST/ALT ratio that had little indicative value for the advanced liver cirrhosis (Figures 1K and 1L), higher serum LECT2 levels were significantly associated with more advanced liver cirrhosis (Figure 1M). Our results suggest that serum LECT2 level may be a potential non-invasive biomarker for liver cirrhosis.

LECT2 Was Expressed by Hepatocytes and Endothelial Cells

To define the cellular source of LECT2 in the liver during fibrogenesis, we examined the colocalization of LECT2 with Alb (hepatocyte marker), CD31 (endothelial marker), α-SMA (activated hepatic stellate cells [HSCs] marker), and CD11b (macrophage marker) in human cirrhotic livers. LECT2 was largely observed in hepatocytes and endothelial cells (ECs) but not in HSCs and macrophages (Figure S1A). In the *Lect2-Cre/Rosa26-Tomato* mice generated in our laboratory, induction of liver fibrosis by CCl4 led to activation of LECT2 transcription in hepatocytes and ECs but not in HSCs or macrophages (Figure S1B). Furthermore, we isolated hepatocytes, ECs, macrophages, and HSCs from the CCl4-induced fibrotic livers of the wild-type (WT) mice to measure the expression patterns of LECT2. Abundant amount of LECT2 was observed in hepatocytes, whereas the other cells (ECs, macrophages, and HSCs) expressed significantly low level of LECT2 (Figures S1C and S1D). *In vitro* studies revealed that transforming growth factor β1 (TGF-β1) could upregulate LECT2 in primary ECs and PHs isolated from WT mice (Figures S1E–S1G).

LECT2 Promoted Liver Fibrosis

To explore whether LECT2 plays crucial roles in liver fibrogenesis, we used the CCl4-induced liver fibrosis model. Consistent with the data from the normal human livers, normal mouse livers expressed low levels of LECT2, mainly around portal vessels and central veins. In contrast, significantly increased expression of LECT2 was observed in the CCl4-induced fibrotic livers, where LECT2 was mostly seen around the portal area and liver injury boundaries (Figures 2A and 2B). It was noteworthy that the extent of increase in the serum LECT2 levels was more significant as compared to that of the serum ALT levels (6- to 7-fold versus 2- to 3-fold) (Figures 2C and 2D).

To test whether LECT2 regulates liver fibrogenesis, mice were injected with lentiviral vector overexpressing LECT2 cDNAs (Lenti-LECT2), and mice injected with empty lentiviral vector (Lenti-V) were used as controls. Overexpression of LECT2 was confirmed in Lenti-LECT2 infected mouse livers and serum samples derived therein (Figures S2A and S2B). Overexpression of LECT2 led to worse liver fibrosis as indicated by stronger Sirius Red staining (Figure 2E). We further used *Lect2* knockout (*Lect2-KO*) mice whose genotype was previously identified (Lu et al., 2016). No hepatic LECT2 expression was observed in *Lect2-KO* mice treated with or without CCl4 (Figures S2C and S2D). Surprisingly, compared to wild-type (WT) littermates, *Lect2-KO* mice exhibited dramatically attenuated fibrosis as measured by Sirius Red staining (Figure 2F). Re-expressing

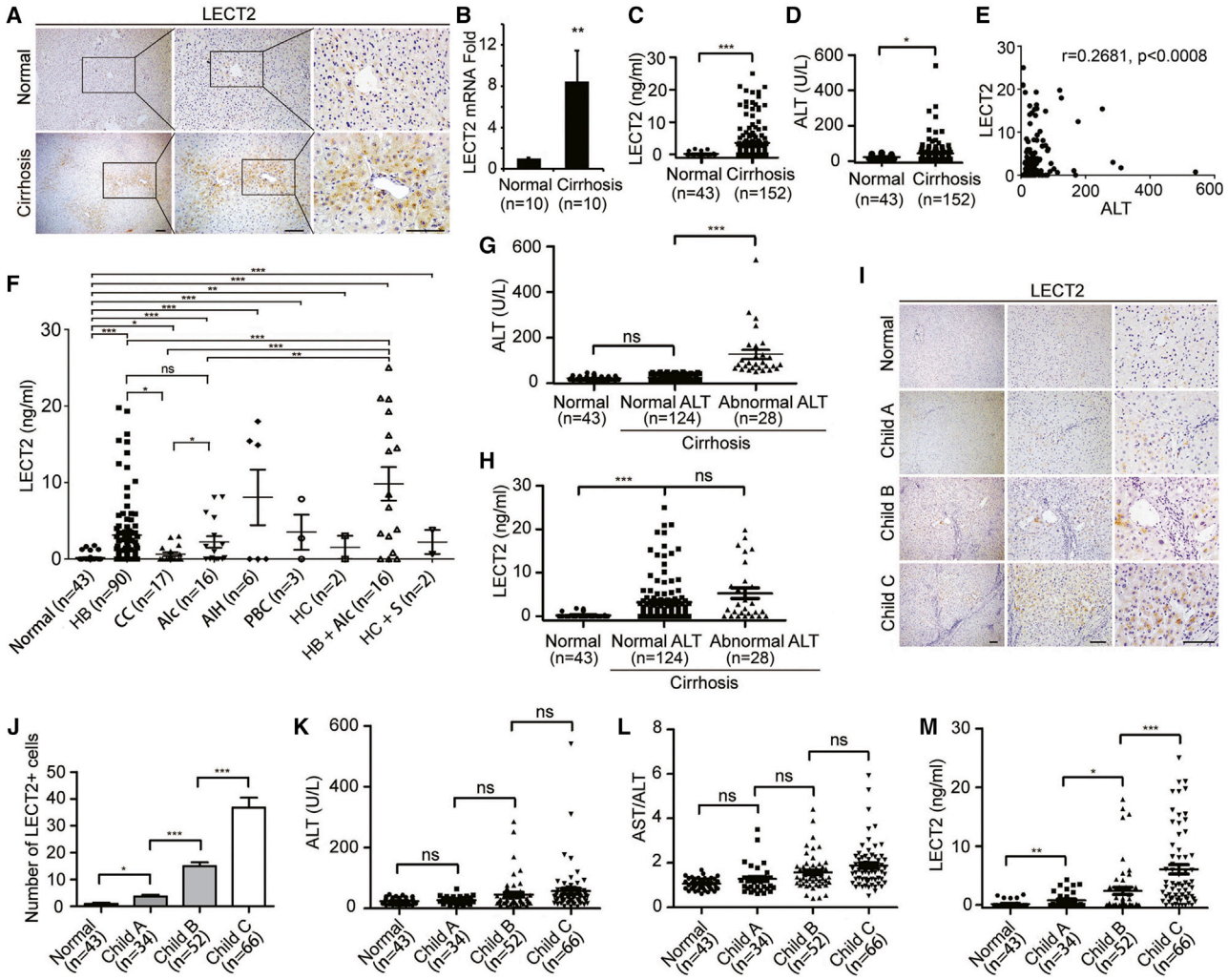

Figure 1. Clinical Significance of LECT2 in Patients with Cirrhosis

(A) Immunohistochemical staining of LECT2 in human normal and cirrhotic liver tissues. Scale bars, 100 μm.

(B) mRNA level of LECT2 in normal and cirrhotic liver.

(C and D) The concentration of the serum LECT2 (C) and ALT (D) in healthy volunteers (normal) and cirrhotic patients (cirrhosis).

(E) The correlation between serum ALT and LECT2 levels in 152 patients with liver cirrhosis was evaluated by Spearman correlation analysis.

(F) Cirrhotic patients were divided into eight different categories according to their etiologies. Hepatitis B-related cirrhosis (HB), cryptogenic cirrhosis (CC), alcoholic cirrhosis (Alc), autoimmune hepatitis-related cirrhosis (AIH), primary biliary cirrhosis (PBC), hepatitis C-related cirrhosis (HC), hepatitis B plus alcoholic cirrhosis (HB + Alc), and hepatitis C plus schistosoma cirrhosis (HC + S).

(G) Cirrhotic patients were divided into two groups: those with normal ALT or those with abnormal ALT.

(H) Serum concentration of LECT2 in healthy people, cirrhotic patients with normal ALT, and cirrhotic patients with abnormal ALT.

(I) Immunohistochemical staining of LECT2 in normal and various grades of cirrhotic livers. Scale bars, 100 μm.

(J) Quantitative analysis of LECT2-positive cells in (H).

(K–M) Serum concentrations of ALT (K), AST/ALT ratio (L), and LECT2 (M) in patients with different grades of cirrhosis. Child-Pugh class A (Child A), Child-Pugh class B (Child B), Child-Pugh class C (Child C). Mean ± SEM. *p < 0.05, **p < 0.01, ***p < 0.001.

See also Figure S1 and Tables S1 and S2.

LECT2 in *Lect2-KO* mice using Lenti-LECT2 (Figure S2E) led to worsened liver fibrosis (Figure 2G).

The above findings were further verified using other mechanistically distinct but complimentary fibrosis models in WT C57BL/6 mice, including bile-duct ligation (BDL)-induced, 3,5-diethoxycarbonyl-1,4-dihydrocollidine (DDC)-induced, and methionine choline deficient diet (MCD)-induced liver fibrosis models. As expected, a significant upregulation of LECT2 was seen in all these models (Figures S2F–S2K), whereas in the above liver fibrosis models established in *Lect2-KO* mice, fibrosis was dramatically attenuated (Figures 2H–2J).

In our studies, we observed that fibrotic factors, α-SMA, TGF-β1, ET1, interleukin (IL)-33, FN1, IL-11, and COL4, were increased in the CCl4-treated Lenti-LECT2 mice, whereas they

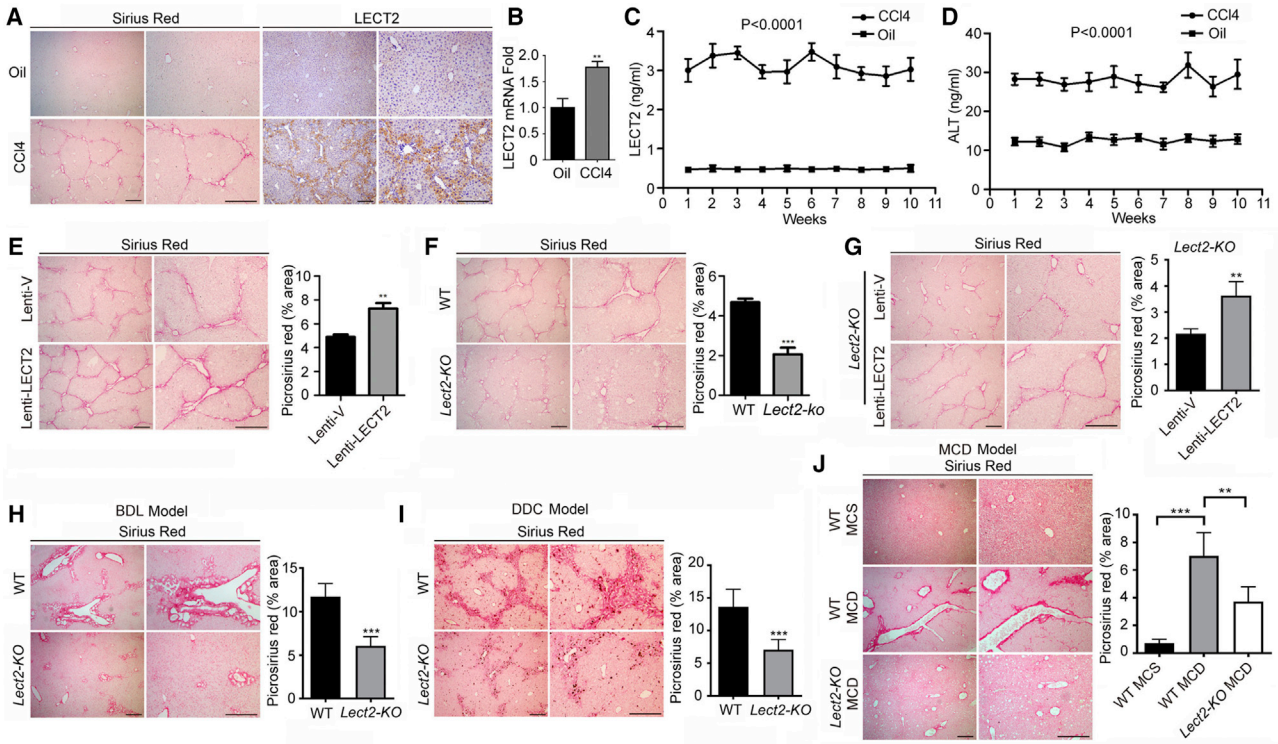

Figure 2. LECT2 Promotes Liver Fibrogenesis

(A) Sirius Red or LECT2 staining in livers of oil controls and CCl4-treated mice.

(B) Hepatic mRNA levels of LECT2.

(C and D) Serum concentrations of LECT2 (C) and ALT (D) in oil controls and CCl4-treated mice.

(E) Liver tissues from Lenti-LECT2-infected (Lenti-LECT2) or Lenti-V-infected (Lenti-V) wild-type (WT) mice with CCl4-induced fibrosis were stained by Sirius Red.

(F) Liver tissues from *Lect2-KO* mice (*Lect2-KO*) or littermate controls with CCl4-induced fibrosis were stained by Sirius Red.

(G) Liver tissues from Lenti-LECT2-infected (Lenti-LECT2) or Lenti-V-infected (Lenti-V) *Lect2-KO* mice with CCl4-induced fibrosis were stained by Sirius Red.

(H–J) Liver fibrosis was induced in *Lect2-KO* mice (*Lect2-KO*) or their littermate controls (WT) by bile duct-ligation (BDL) (H), DDC treatment (I), and MCD diet (J). Liver tissues from each group were stained by Sirius Red. In all animal studies, n = 6/group. In all panels, scale bars, 200 μm. Mean ± SEM. $^{**}p < 0.01$, $^{***}p < 0.001$. See also Figure S2.

decreased in the *Lect2-KO* mice (Figures S2L and S2M). Lenti-LECT2 rescued the expression of these fibrotic factors in *Lect2-KO* mice with CCl4-induced liver fibrosis (Figure S2N). Furthermore, there was a widespread reduction in the mRNA expression of these fibrotic factors in BDL-, DDC-, and MCD-induced liver fibrosis in *Lect2-KO* mice, compared to the control mice (Figures S2O–S2Q).

To confirm that LECT2 regulated EC to secrete these fibrotic factors, the immortalized vascular endothelial cell line EA.hy926 was employed for our *in vitro* studies. Treatment of the EA.hy926 cells with rLECT2 enhanced the mRNA levels of fibrotic factors but decreased the mRNA level of eNOS (Figure S2R). On the contrary, LECT2 knockdown by small interfering RNAs (siRNAs) (Figure S2S) reversed these effects (Figure S2T).

LECT2 Functioned as an Anti-angiogenic Factor *In Vitro* and *In Vivo*

We next explored how LECT2 regulated the development of liver fibrosis. Given the important role of angiogenesis in liver fibrosis and considering the expression pattern of LECT2 in blood vessels, we speculated that LECT2 may be mechanistically involved in the biological functions of EC. Indeed, we observed that rLECT2 inhibited the migration and tube formation of EA.hy926 cells (Figures 3A and 3B), whereas knocking down of LECT2 reversed these effects (Figures 3C and 3D). Furthermore, we found that LECT2 siRNAs did not alter the migration and tube formation of EA.hy926/LECT2-siRNA-resistant cells (Figures S3A and S3B).

We further isolated primary hepatocytes (PH), liver sinusoid endothelial cells (LSEC), and HSCs from WT and *Lect2-KO* mice. We found that rLECT2 inhibited the migration and tube formation of the LSECs isolated from WT mice (Figures 3E and 3F). When co-cultured with LSECs, PHs from WT, but not *Lect2-KO*, mice inhibited the migration and tube formation of the LSCEs (Figures S3C and S3D). The condition media from the LSECs co-cultured with PHs from WT mice, but not with PHs from the *Lect2-KO* mice, promoted the expression of α-SMA in HSCs (Figure S3E).

In CCl4-induced liver fibrosis model, overexpression of LECT2 by Lenti-LECT2 led to significant decrease in the number of $CD31^+$ vessels (a reliable marker for angiogenesis) surrounding the portal area (Figures 3G, left and middle, and 3H). In contrast,

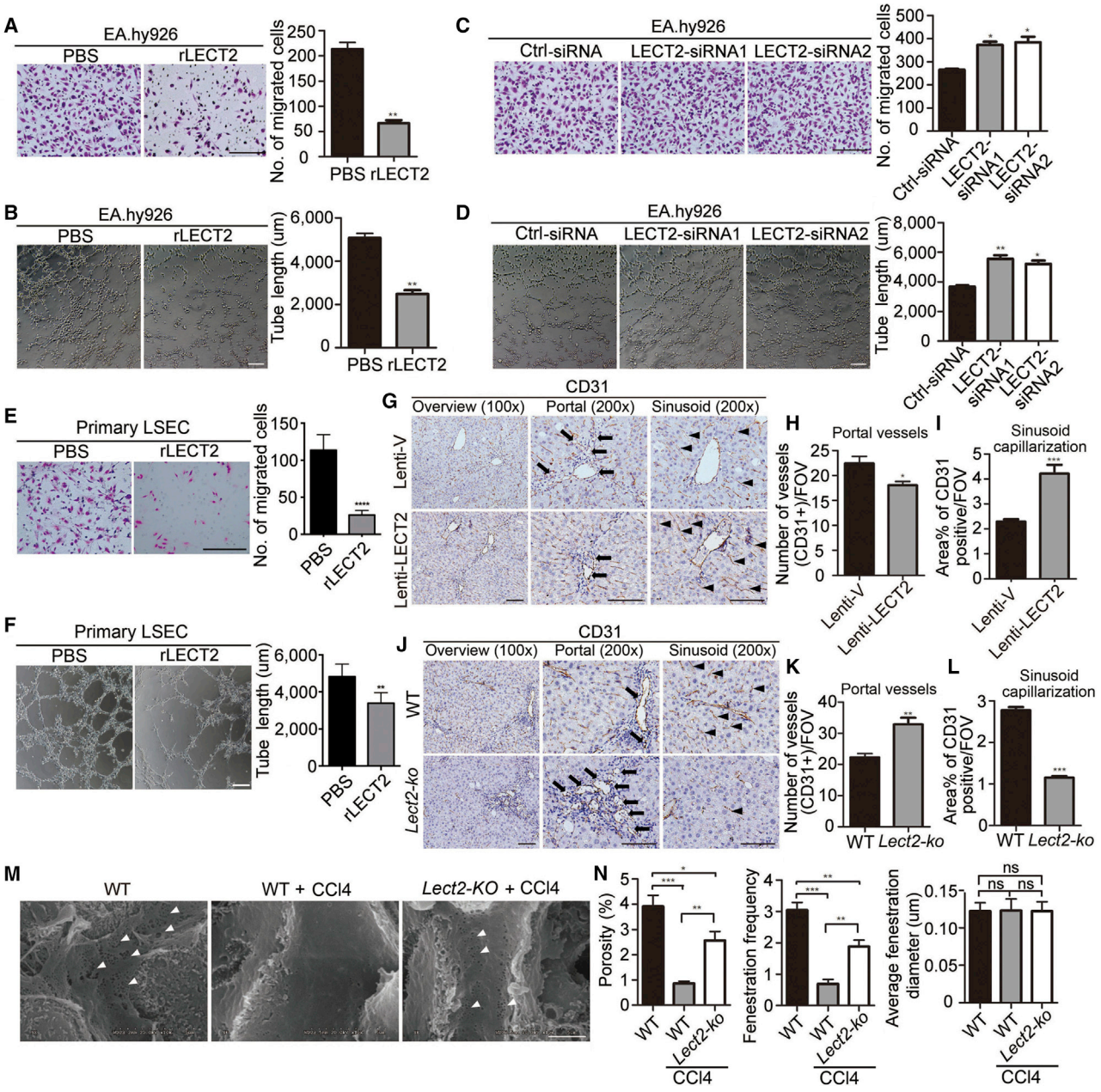

Figure 3. LECT2 Regulates EC Migration, Tube Formation, Portal Angiogenesis, and Sinusoid Capillarization

(A) LECT2 inhibited the migration of EA.hy926 cell. Scale bar, 100 μm.

(B) LECT2 inhibited tube formation of EA.hy926 cell. Scale bar, 200 μm.

(C) Inhibition of LECT2 enhanced migration of EA.hy926 cell. Scale bar, 100 μm.

(D) Inhibition of LECT2 enhanced tube formation of EA.hy926 cell. Scale bar, 200 μm.

(E) LECT2 inhibited the migration of primary liver sinusoid endothelial cell (LSEC). Scale bar, 100 μm.

(F) LECT2 inhibited tube formation of primary LSEC. Scale bar, 200 μm.

(G) Liver tissues were immunohistochemically stained for CD31. Arrows indicate portal vessels, and arrowheads indicate capillarization of liver sinusoids. Scale bar, 200 μm.

(H) The number of CD31-positive vessels surrounding the portal area was measured.

(I) The CD31-positive capillarization of liver sinusoids was measured.

(J) Liver tissues were immunohistochemically stained for CD31. Arrows indicate portal vessels, and arrowheads indicate capillarization of liver sinusoids. Scale bar, 200 μm.

(K) The number of CD31-positive vessels surrounding the portal area was measured.

(L) The CD31-positive capillarization of liver sinusoids was measured.

(legend continued on next page)

in CCl4-induced liver fibrosis model in *Lect2-KO* mice, a significant increase in the number of $CD31^+$ vessels was seen around the portal area (Figures 3J, left and middle, and 3K). In BDL-, DDC-, and MCD-induced liver fibrosis models in *Lect2-KO* mice, a significantly increased number of $CD31^+$ blood vessels was also observed surrounding the portal area as compared to the WT littermates' livers (Figures S3F–S3N). Co-staining for LECT2 and VEGFR2 in CCl4-induced fibrotic livers of WT mice and patients' cirrhotic livers revealed few VEGFR2-positive vessels in $LECT2^{high}$ expression area, whereas numerous VEGFR2-positive vessels were seen in $LECT2^{low}$ expression area (Figure S3O). More CD31 and VEGFR2 double-positive vessels ($CD31^+/VEGFR2^+$) were seen in the portal areas of the fibrotic livers from *Lect2-KO* mice, as compared to the WT control mice (Figure S3P). These data indicated an anti-angiogenic role of LECT2.

LECT2 Promoted Capillarization of Liver Sinusoids

An interesting finding in the above studies was that decreased angiogenesis surrounding the portal area in LECT2 overexpressing mice of CCl4-induced liver fibrosis model was associated with a significantly increased capillarization of liver sinusoids (Figures 3G, right, and 3I). In contrast, decreased capillarization of liver sinusoids was seen in the CCl4-induced fibrotic livers of *Lect2-KO* mice (Figures 3J, right, and 3L). In BDL-, DDC-, and MCD-induced liver fibrosis models, decreased capillarizations of sinusoids were observed in the livers of *Lect2-KO* mice as compared to the WT littermates' livers (Figures S3F–S3N). As capillarization of the sinusoids results in a distorted structure of hepatic sinusoids and loss of specific endothelial fenestration, we examined the level of fenestration in the mouse livers of CCl4-induced liver fibrosis models using scanning electron microscopy. As shown in Figures 3M and 3N, LSECs from WT mice lost their fenestration whereas LSECs from *Lect2-KO* mice regained fenestration.

Direct Interaction between LECT2 and Tie1

We next explored the mechanism of how LECT2 regulated EC functions. It was previously reported that the orphan EC receptor Tie1 was a candidate receptor for LECT2 (Chen et al., 2014). In our studies, abundant expression of Tie1 was seen in the isolated ECs but not the PHs, macrophages, and HSCs (Figures S3Q and S3R).

To clarify the interaction between LECT2 and Tie1, we found that LECT2 co-localized with Tie1 in portal vessels of cirrhotic livers of both human and mouse origins (Figure S3S). To confirm these initial findings, we employed various truncations of Tie1 fused with Flag-tag and truncations of LECT2 fused with Myc-tag (Figure 4A). By co-immunoprecipitation (coIP) experiments, the interactions between exogenously expressed Myc-tagged LECT2 and Flag-tagged Tie1 were confirmed in 293T cells (Figure 4B), and the interactions between endogenously expressed LECT2 and Tie1 were confirmed in EA.hy926 cells (Figure 4C). The interactions between rLECT2 and endogenous Tie1 were also detected (Figure 4D). Here, LECT2 was not co-immunoprecipitated with Tie2 (Figure S3T).

To investigate which domain of Tie1 is crucial for LECT2 binding, various Tie1 truncations together with LECT2 cDNAs were transfected into 293T cells. Using coIP experiments, we first demonstrated LECT2 co-immunoprecipitated with N terminus of the extracellular domains of Tie1 (Figure 4E). We further found that LECT2 co-immunoprecipitated with the Ig3 domain of Tie1 (Figure 4F). To investigate whether LECT2 binds to Tie1 directly, we purified Ig3 domain of human Tie1 protein with an N-terminal Maltose binding protein (MBP) tag. Using purified proteins of rLECT2 and MBP-Tie1-Ig3, we performed MBP beads Pull-Down assay and found that rLECT2 bound to MBP-Tie1-Ig3, but not MBP (Figure 4G).

To measure the binding affinity between LECT2 and Tie1, we employed a surface plasmon resonance (SPR) assay and obtained a K_d value of 0.52 μM for these two proteins (Figure 4H). Their interaction showed a "slow-disassociation" pattern. MBP protein control displayed a much weaker response compared to MBP-tagged Tie1 protein at a similar concentration (Figure 4I).

To explore whether the Ig3 domain of Tie1 is essential for LECT2-Tie1 interaction, a Tie1 mutation that lacks the Ig3 domain (Tie1-δIg3) was constructed (Figure 4A). CoIP experiments showed that LECT2 interacted with WT Tie1, but not with Tie1-δIg3 (Figure 4J). Furthermore, we re-expressed WT Tie1 or Tie1-δIg3 into Tie1 knockdown EA.hy926 cells. LECT2 failed to regulate the migration and tube formation of EA.hy926 cells transfected with Tie1-δIg3 (Figures 4K and 4L).

We then clarified how LECT2 binds to Tie1. We adopted the cross-linking coupled with mass spectrometry (XL-MS) technique to map the surface regions of the two proteins involved in their direct interactions and built an interaction model of these two proteins (Figure 4M; Table S3). Interestingly, when we used a multi-domain Tie1 model derived from the crystal structure of Tie2 containing the Ig1, Ig2, EGF, and Ig3 domains (Barton et al., 2006), the proposed interface between Tie1 Ig3 and LECT2 was just on the other side of the interface between Ig3 and other Tie1 domains (Figure 4N). This result suggests that the manner in which LECT2 protein interacts with multi-domain (even full-length) Tie1 may be similar to how it interacts with the single Ig3 domain of Tie1 as we modeled based on the XL-MS data.

To validate this proposed interaction model between Tie1 and LECT2 (Figure 4O), we further mapped that aa360–aa377 of Tie1 was necessary for the interaction between Tie1 and LECT2 (Figure 4P). As summarized in Figure 4S, two substitutions (1 and 2) of Tie1 residues by corresponding Tie2 residues dramatically reduced their binding to LECT2 (Figures 4Q and 4R). These results not only validate our interaction model, but also suggest that these specific interface residues of Tie1 (sequence alignment of Tie1 and Tie2) may be responsible for the recognition by LECT2, which does not bind to Tie2.

(M) Scanning electron micrographs showing the hepatic sinusoids in the liver tissues from normal C57BL/6 mice (WT), WT C57BL/6 mice treated with CCl4 (WT + CCl4), and *Lect2-KO* mice treated with CCl4 (*Lect2-KO* + CCl4). Arrows, LSEC fenestrae. Scale bar, 2.5 μm.

(N) Porosity, fenestration frequency, and average fenestration diameter were analyzed by ImageJ. Mean ± SEM. *$p < 0.05$, **$p < 0.01$, ***$p < 0.001$.

See also Figure S3.

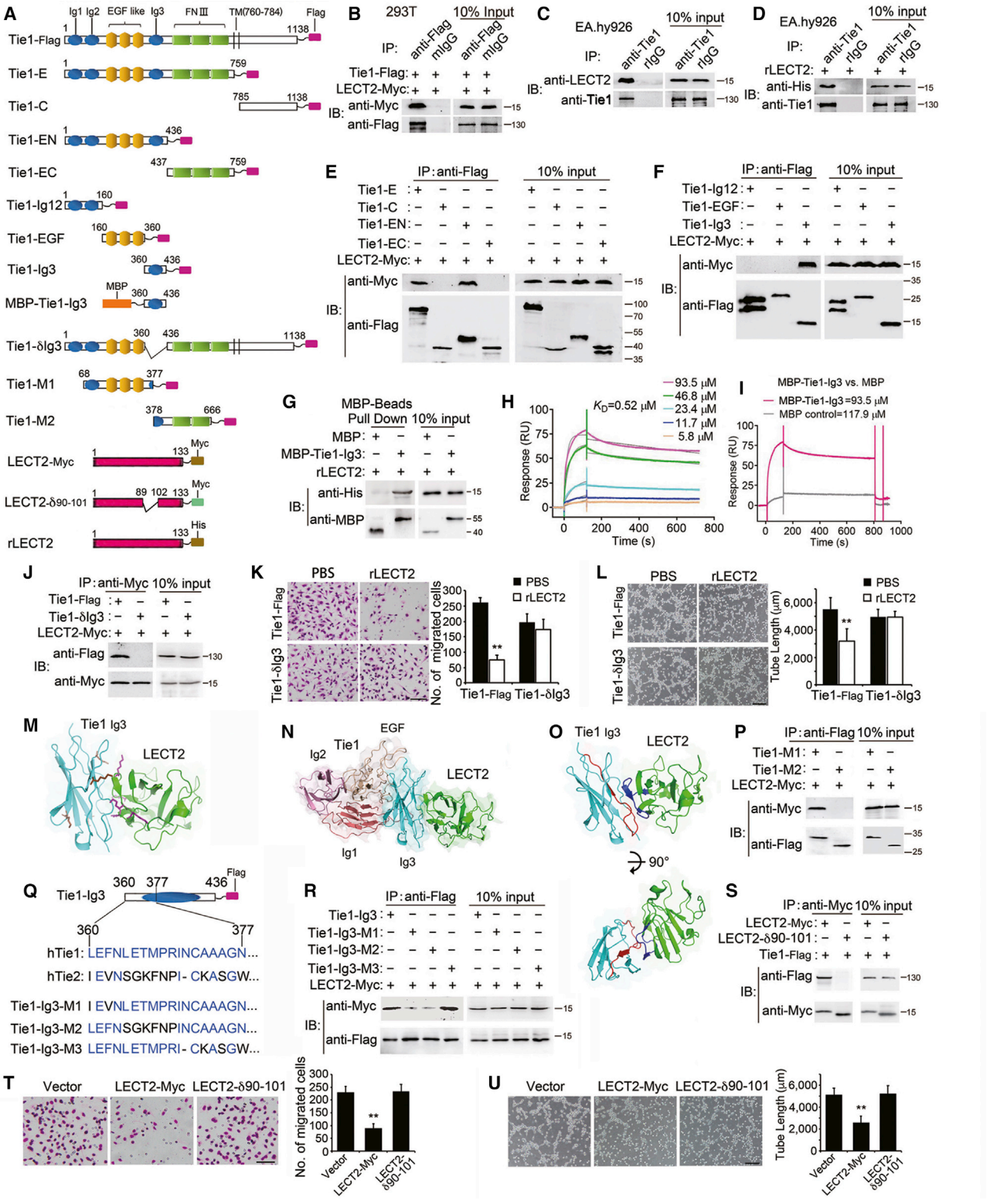

Figure 4. Direct Interactions between LECT2 and Tie1

(A) Schematic illustration of Tie1 and LECT2 constructs.

(B) Exogenous Myc-tagged LECT2 and Flag-tagged Tie1 were immunoprecipitated.

(C) Endogenous LECT2 and Tie1 were immunoprecipitated.

(legend continued on next page)

For LECT2, we deleted aa90–aa101 to generate a mutant of LECT2 (LECT2-δ90-101) based on the interaction model of Tie1 and LECT2 (Figures 4A and 4O). Using a coIP experiment, LECT2-δ90-101 could not interact with Tie1 (Figure 4S). Using functional assays, we found that WT LECT2, but not LECT2-δ90-101, significantly inhibited the migration and tube formation of the EA.hy926 cells (Figures 4T and 4U).

LECT2 Dissociated Tie1/Tie2 Heterodimers and Promoted Tie2/Tie2 Homodimers

Tie1/Tie2 heterodimerization is critical for their downstream signal transmission (Saharinen et al., 2005; Seegar et al., 2010). We next asked whether LECT2/Tie1 interaction affected Tie1/Tie2 association. Using coIP assays, we found that rLECT2 inhibited Tie1/Tie2 association (Figure 5A). Large BiT (LgBiT) and Small BiT (SmBiT) subunits were fused to Tie1 or Tie2 using NanoBiT protein:protein interactions system (Figure 5B). We found that the luminescent signal was reduced by rLECT2 in a dose-dependent manner (Figures 5C and S4A). We then evaluated Tie1/Tie1 and Tie2/Tie2 interactions using the same NanoBiT system (Figures S4B) and found that rLECT2 decreased Tie1/Tie2 heterodimers and increased Tie2/Tie2 homodimers, whereas Tie1/Tie1 homodimers were not affected by rLECT2 (Figure 5D). Furthermore, both rLECT2 protein and overexpression of LECT2 promoted the phosphorylation of Tie2 and MAPK p38, but inhibited the phosphorylation of Tie1 (Figures 5E and S4C). Knock down of LECT2 has the opposite effects (Figures 5F and S4D). The phosphorylation of Tie2 by LECT2 was both dose- and time-dependent (Figures 5E and S4E). Modulation of LECT2 by rLECT2, Lenti-LECT2, and LECT2 siRNA also altered the total Tie2 levels (Figures 5E, 5F, and S4C–S4E), suggesting that Tie2 proteins may be more stable in Tie2/Tie2 homodimers than in Tie1/Tie2 heterodimers. To verify this hypothesis, EA.hy926 cells were pre-treated with MG-132 (a proteasome inhibitor) or CHX (a protein synthesis inhibitor) followed by treatment with rLECT2. We found that rLECT2 did not increase Tie2 in the MG-132 pre-treated EA.hy926 cells (Figure S4F), but inhibited the degradation of Tie2 in the EAhy.926 cells pre-treated with CHX (Figures S4G and S4H).

Tie1 Was Required for LECT2 to Exert Functional Impacts on ECs during Liver Fibrogenesis

To investigate whether Tie1 was required for LECT2 to regulate the migration and tube formation of ECs, we generated two stable Tie1 knockdown cell lines (EA.hy926/Tie1-shRNA1 and EA.hy926/Tie1-shRNA2) using lentiviral Tie1-shRNA (Figure S4I). We found that rLECT2 only inhibited migration and tube formation of the EA.hy926/Ctrl-shRNA cells but not the Tie1 knockdown cells (Figures 5G and 5H). rLECT2 dramatically changed the expression of fibrotic factors in EA.hy926/Ctrl-shRNA cells but not in Tie1 knockdown cells (Figure S4J). We re-expressed Tie1-WT, kinase-dead mutant of Tie1 (Tie1-K870R), and Tie1-δIg3 in the Tie1 knock down EA.hy926 cells (Figure S4K). We found that rLECT2 dramatically inhibited migration and tube formation of EA.hy926/Tie1-WT cells, but not EA.hy926/Tie1-K870R and EA.hy926/Tie1-δIg3 cells (Figures 5I and 5J). We knocked down Tie2 and found that rLECT2 could dramatically inhibit the migration and tube formation of the EA.hy926/Ctrl-shRNA cells but not the Tie2 knockdown cells (Figures S4L–S4N).

To investigate whether Tie1 was required for LECT2 to regulate liver fibrosis and angiogenesis/sinusoid capillarization *in vivo*, endogenous Tie1 was knocked down by injecting adenoviral Tie1-shRNA (Figure 5K). Tie1 knockdown worsened the liver fibrosis, inhibited portal angiogenesis, but increased liver sinusoid capillarization (Figures 5L–5O). In mice with CCl4-induced liver fibrosis and Tie1 knockdown, overexpression of LECT2 neither affected the level of fibrosis (Figure 5P), nor affected the level of portal angiogenesis and capillarization of liver sinusoids (Figures 5Q–5S). The expression levels of the fibrotic factors were also not changed (Figure S4O).

LECT2 was reported to bind to Met (Chen et al., 2014), VEGFR2 (Chen et al., 2016), and CD209a (Lu et al., 2013). However, in our studies, knockdown of VEGFR2 (Figure S4P)

(D) rLECT2 and endogenous Tie1 were immunoprecipitated.
(E) LECT2 bound to Tie1-E and Tie1-EN.
(F) LECT2 bound to Tie1-Ig3.
(G) Direct binding of rLECT2 to rTie1-Ig3 using MBP pull down assay.
(H and I) Measurement of the binding affinity between LECT2 and Tie1 proteins by SPR method. (H) Representative sensorgrams obtained at different concentrations of Tie1 protein. (I) Sensorgram comparison between MBP-tagged Tie1 protein and MBP control.
(J) LECT2 could not bind to Tie1-δIg3.
(K) Transwell assay was performed in the absence or presence of rLECT2, and the numbers of migrated cells were measured. Scale bar, 100 μm.
(L) Tube formation assay was performed in the absence or presence of rLECT2, and the tube lengths were measured. Scale bar, 200 μm.
(M) Proposed interface between Tie1 Ig3 domain and LECT2 protein based on the XL-MS data.
(N) Modeled interaction between LECT2 and multi-domain Tie1 protein, using the crystal structure of Tie2 (PDB: 2GY5) as a template.
(O) The surface regions of Tie1 and LECT2 proteins involved in their modeled interaction (red for Tie1 aa360–aa377 and blue for LECT2 aa90–aa101) and chosen for validation by mutagenesis.
(P) LECT2 interacted with Tie1-M1 but not Tie1-M2.
(Q) The sequences of Tie1 Ig3 region aa360–aa377 and the substitutions in three mutants by corresponding Tie2 residues: Tie1-Ig3-M1(L360I, F360V), Tie1-Ig3-M2 (L364S, E365G, T366K, M367F, P368N, R369P), and Tie1-Ig3-M3 (δN371, A373K, A375S, N377W).
(R) LECT2 interacted strongly with Tie1-Ig3 and Tie1-Ig3-M3 and weakly with Tie1-Ig3-M1 and Tie1-Ig3-M2.
(S) Tie1 interacted with LECT2-myc, but not LECT2-δ90-101.
(T and U) EA.hy926 cells were transfected with control vector, full-length LECT2 (LECT2-Myc), or LECT2-δ90-101. Transwell assay was performed, and the numbers of migrated cells were measured (T). Scale bar, 100 μm. Tube formation assay was performed, and the tube lengths were measured (U). Scale bar, 200 μm. Mean ± SEM. *$p < 0.05$, **$p < 0.01$.
See also Figure S3 and Table S3.

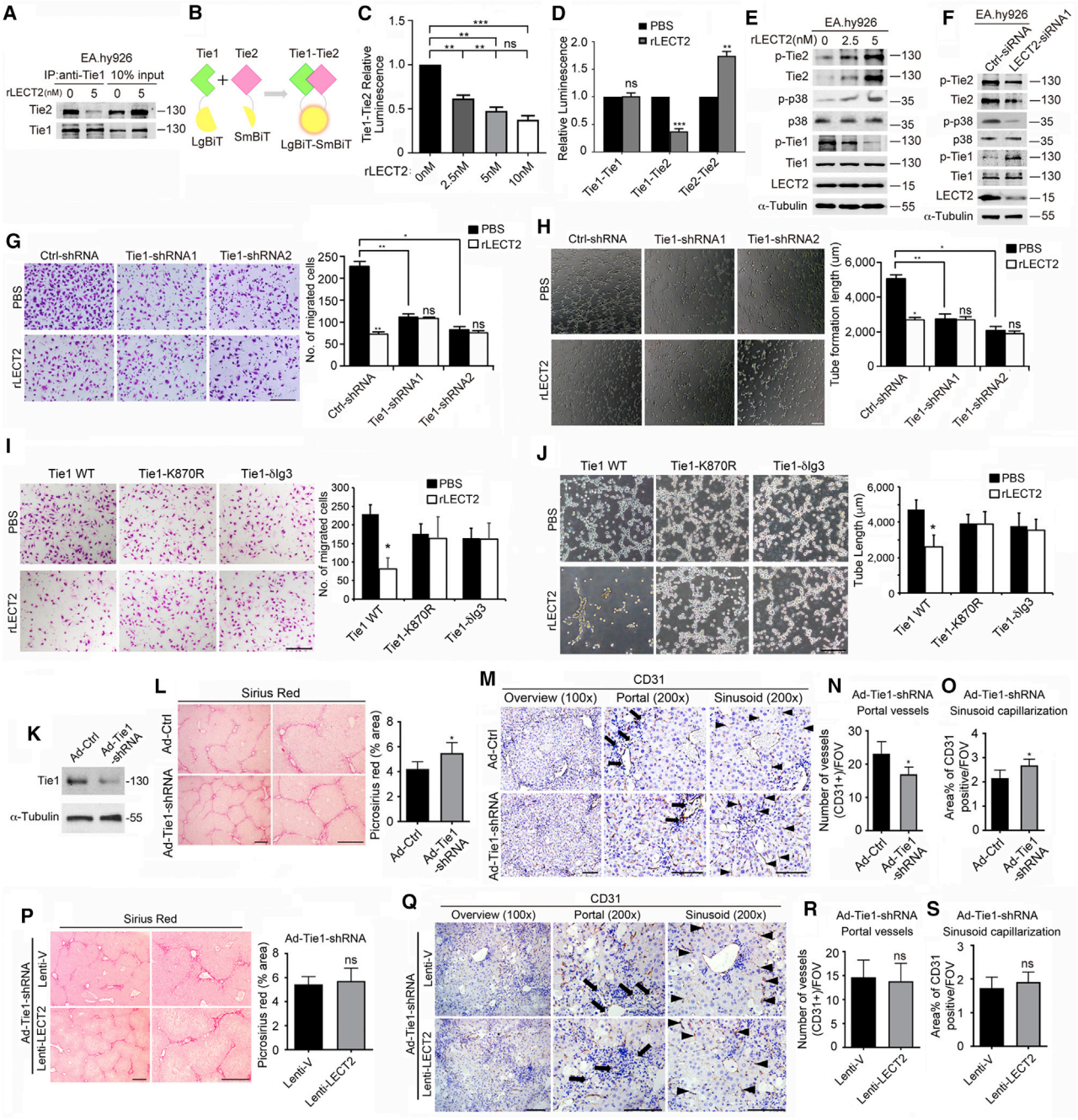

Figure 5. LECT2 Interrupts Tie1/Tie2 Interactions and Regulates EC Functions and Liver Fibrogenesis through Tie1

(A) LECT2 interrupted endogenous Tie1/Tie2 interactions in EA.hy926 cells using coIP assay.

(B) Schematic illustration of NanoBiT protein:protein interactions system.

(C) rLECT2 reduced luminescent signal of Tie1/Tie2 interactions.

(D) rLECT2 reduced luminescent signal of Tie1/Tie2 interactions and increased luminescent signal of Tie2/Tie2 interactions.

(E) rLECT2 increased Tie2 phosphorylation and total Tie2 levels, increased p38 phosphorylation, and reduced Tie1 phosphorylation.

(F) Knockdown of LECT2 reduced Tie2 phosphorylation and total Tie2 levels, reduced p38 phosphorylation, and increased Tie1 phosphorylation.

(G) rLECT2 failed to inhibit the migration of EA.hy926 cells with Tie1 knockdown.

(H) rLECT2 failed to inhibit tube formation of EA.hy926 cells with Tie1 knockdown.

(I and J) Stable EA.hy926 cells with Tie1 knockdown were transfected with wild-type Tie1 (Tie1-WT), kinase dead mutant of Tie1 (Tie1-K870R), or Ig3 deletion mutant of Tie1 (Tie1-δIg3). (I) rLECT2 inhibited the migration of EA.hy926/Tie1-WT cells but not EA.hy926/Tie1-K870R cells and EA.hy926/Tie1-δIg3 cells. (J) rLECT2 inhibited tube formation of EA.hy926/Tie1-WT cells but not EA.hy926/Tie1-K870R cells and EA.hy926/Tie1-δIg3 cells.

(K) Wild-type (WT) mice infected with Ad-Tie1-shRNA or Ad-Ctrl-shRNA; the expression of Tie1 in the liver was detected by immunoblotting.

(legend continued on next page)

did not affect the inhibitory effect of rLECT2 on the migration and tube formation of EA.hy926 cells (Figures S4Q and S4R). Similar results were obtained when the phosphorylation of Met and VEGFR2 in EA.hy926 cells was inhibited by golvatinib (an inhibitor for Met and VEGFR2) or vandetanib (an inhibitor for VEGFR2) (Figures S4S–S4W), or when CD209a was knocked down (Figures S4X–S4Z).

In vivo knockdown of endogenous VEGFR2 (Figure S5A) followed by LECT2 overexpression led to worsened liver fibrosis (Figure S5B), increased fibrotic factors (Figure S5C), reduced portal angiogenesis, and increased liver sinusoid capillarization (Figures S5D–S5F). In *Lect2-KO* mice, inhibition of VEGF/VEGFR by their inhibitors sorafenib and bevacizumab attenuated liver fibrosis (Figure S5G). These results indicated that LECT2 and VEGF/VEGFR are independent of each other. When the endogenous CD209a was knocked down (Figure S5H), LECT2 overexpression was still able to worsen liver fibrosis (Figure S5I), upregulate the expression levels of fibrotic factors (Figure S5J), inhibit portal angiogenesis, and increase liver sinusoid capillarization (Figures S5K–S5M).

Taken together, these results demonstrated that LECT2 regulates EC functions and liver fibrogenesis through Tie1 but not Met, VEGFR2, or CD209a.

LECT2 Regulated PPAR Signaling Pathway

To explore the mechanisms underlying the regulatory effects of LECT2 on liver fibrosis, RNA sequencing (RNA-seq) analysis was performed on CCl4-induced fibrotic liver samples derived from *Lect2-KO* and control WT C57/BL mice. A total of 689 genes differentially expressed in liver tissues (with a p value < 0.05 and a fold change >2) were identified (Figure S6A; Table S4). By Kyoto Encyclopedia of Genes and Genomes (KEGG) pathway enrichment analysis, these genes were mainly categorized into metabolism, biosynthesis, cell cycle, DNA replication, chemical carcinogenesis, PPAR signaling pathway, and p53 signaling pathway (Figure 6A).

Peroxisome proliferator-activated receptors (PPARs) are nuclear receptors that belong to the steroid hormone receptor superfamily, including three isoforms: PPARα, PPARβ, and PPARγ (Berger and Moller, 2002). A significant upregulation of PPARγ was observed in fibrotic livers (Figure S6B). We observed that treatment of EA.hy926 cells and primary LSECs with rLECT2 caused a significant upregulation of PPARγ but not PPARα and PPARβ (Figures 6B and 6C). To explore whether LECT2 upregulated PPARγ through Tie1, we re-expressed Tie1-WT or Tie1-δIg3 into Tie1 knockdown EAhy926 cells and found that rLECT2 could not increase the expression of PPARγ in EA.hy926/Tie1-δIg3 cells, while LECT2 significantly increased the expression of PPARγ in EA.hy926/Tie1-WT cells (Figure S6D). In addition, we found that inhibition of PPARγ by GW9662 (a specific PPARγ inhibitor; Fujii et al., 2012) reversed the effects of rLECT2 on migration and tube formation (Figures 6E and 6F) and the production of fibrotic factors (Figure S6C) in EAhy.926 cells.

Degradation of the extracellular matrix is a necessary step during the early stages of angiogenesis. Matrix metalloproteinases (MMPs) produced by ECs are involved in capillary growth and can be downregulated by PPARγ agonists (Huang et al., 2009; Tyagi et al., 2006). To explore whether MMPs were regulated by LECT2, we analyzed RNA-seq data and found that MMP2, MMP7, MMP12, and MMP13 were significantly upregulated in the fibrotic liver tissues derived from *Lect2-KO* mice (Figure S6D). We further found that rLECT2 decreased the expression of MMP2, MMP7, MMP12, and MMP13, and these effects could be rescued by PPARγ inhibitor GW9662 (Figures 6G and 6H). Downregulation of MMPs was also observed in fibrotic livers (Figure S6E). MMP7 has been reported to promote cell migration by degrading VE-cadherin (Ichikawa et al., 2006). We found that treatment of EA.hy926 cells and primary LSECs by rLECT2 led to increased expression of VE-cadherin, and this could be reversed by GW9662 and MAPK p38 inhibitor SB203580 (Figures 6I and 6J). Hence, through our results, we proposed that LECT2-Tie1 is an important signaling pathway in promoting liver fibrogenesis through MAPK/PPAR/MMP/VE-cadherin, as illustrated in Figure S6F.

AAV9-LECT2 shRNA Attenuated Liver Fibrosis

Our data indicate that LECT2 inhibition might represent a valuable therapeutic approach for liver fibrosis. Because adeno-associated viral (AAV) system has been proved to be safe for therapeutic payload delivery, we used AAV9 vectors to deliver LECT2 shRNA to mice with CCl4-induced fibrosis. Thus, AAV9-LECT2 shRNA or control (AAV9-Ctrl shRNA) were injected into C57BL/6 mice, followed by CCl4 injections twice weekly for 3 weeks (Figure 7A). A significant reduction in the hepatic expression of LECT2 was seen in the mice treated with AAV9-LECT2 shRNA (Figures S7A–S7D), together with much attenuated liver fibrosis (Figure 7B) and significant reduction in mRNA expression of fibrotic factors (Figure 7C). Increased portal angiogenesis and decreased capillarization of the sinusoids were also observed in AAV9-LECT2 shRNA-infected mice (Figures 7D–7F). In addition, increased frequency of open fenestrae in LSECs was seen in AAV9-LECT2 shRNA but not control mice (Figures 7G and 7H).

(L) Liver tissues from Ad-Tie1-shRNA- or Ad-Ctrl-shRNA-infected mice with CCl4-induced fibrosis were stained with Sirius Red. Scale bar, 200 μm.
(M) Liver tissues were immunohistochemically stained for CD31. Arrows indicate portal vessels, and arrowheads indicate capillarization of liver sinusoids. Scale bar, 200 μm.
(N) The CD31-positive vessels surrounding the portal area were measured.
(O) The CD31-positive capillarization of liver sinusoids was measured.
(P) Liver tissues from Ad-Tie1-shRNA- and Lenti-LECT2- or Lenti-V-infected mice with CCl4-induced fibrosis were stained with Sirius Red. Scale bar, 200 μm.
(Q) Liver tissues were immunohistochemically stained for CD31. Arrows indicate portal vessels, and arrowheads indicate capillarization of liver sinusoids. Scale bar, 200 μm.
(R) The CD31-positive vessels surrounding the portal area were measured.
(S) The CD31-positive capillarization of liver sinusoids was measured. Mean ± SEM. *p <0.05, **p <0.01, ***p <0.001.
See also Figures S4 and S5.

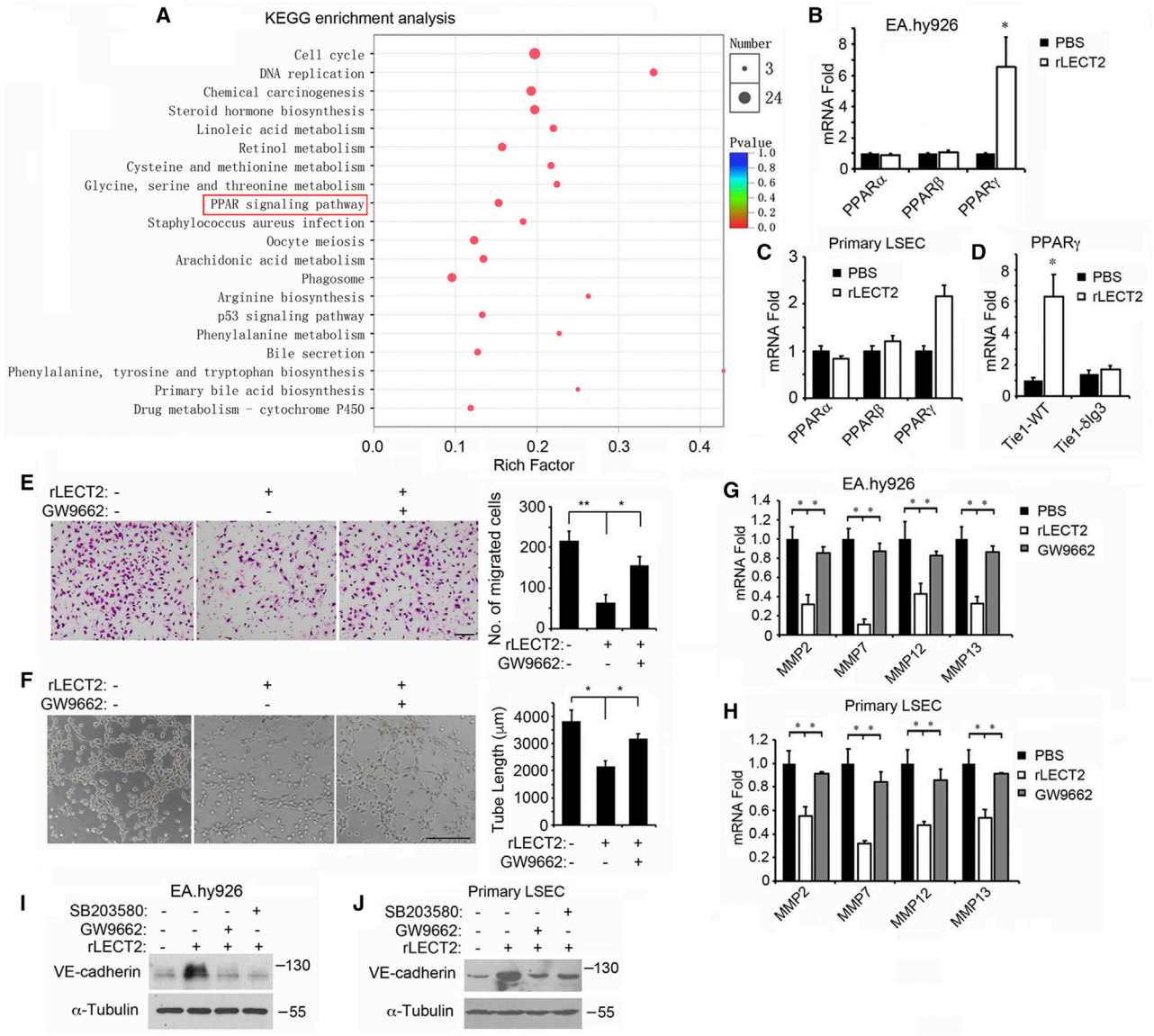

Figure 6. LECT2-Tie1 Activates PPAR Signaling Pathway

(A) KEGG pathway enrichment analysis.

(B and C) mRNA levels of PPARα, PPARβ, and PPARγ in EA.hy926 cells (B) and primary LSECs (C).

(D) mRNA levels of PPARγ in EA.hy926/Tie1-WT cells and EA.hy926/Tie1-δIg3 cells.

(E and F) PPARγ inhibitor GW9662 reversed the effects of rLECT2 on EA.hy926 cell migration (E) and tube formation (F). Scale bar, 200 μm.

(G and H) rLECT2 inhibited the expression of MMPs, whereas GW9662 reversed the expression of MMPs in EA.hy926 cells (G) and primary LSECs (H).

(I and J) LECT2 increased the expression of VE-cadherin, whereas GW9662 and MAPK inhibitor SB203580 reversed the expression of VE-cadherin in EA.hy926 cells (I) and primary LSECs (J). Mean ± SEM. *$p < 0.05$, **$p < 0.01$, ****$p < 0.0001$.

See also Figure S6 and Table S4.

Finally, we asked whether AAV9-LECT2 shRNA could prevent the further progression of established fibrosis. This experiment was designed as illustrated in Figure 6I. Treatment of mice with AAV9-LECT2 shRNA significantly reduced the hepatic expression of LECT2 (Figures S7E–S7H), attenuated liver fibrosis (Figure 7J), and reduced the mRNA levels of fibrotic factors (Figure 7K). Increased portal angiogenesis and decreased capillarization of the sinusoids were observed in AAV9-LECT2 shRNA-treated mice as compared to the control mice (Figures 7L–7N).

Thus, our findings suggest that inhibition of LECT2 may be of potential value in the treatment of liver fibrosis.

DISCUSSION

Tie1 remained a mechanistically poorly characterized EC-specific orphan receptor thus far. Using multiple complementary approaches, we identified that LECT2 directly binds to the Ig3 domain of Tie1, leading to a shift from Tie1/Tie2 heterodimers

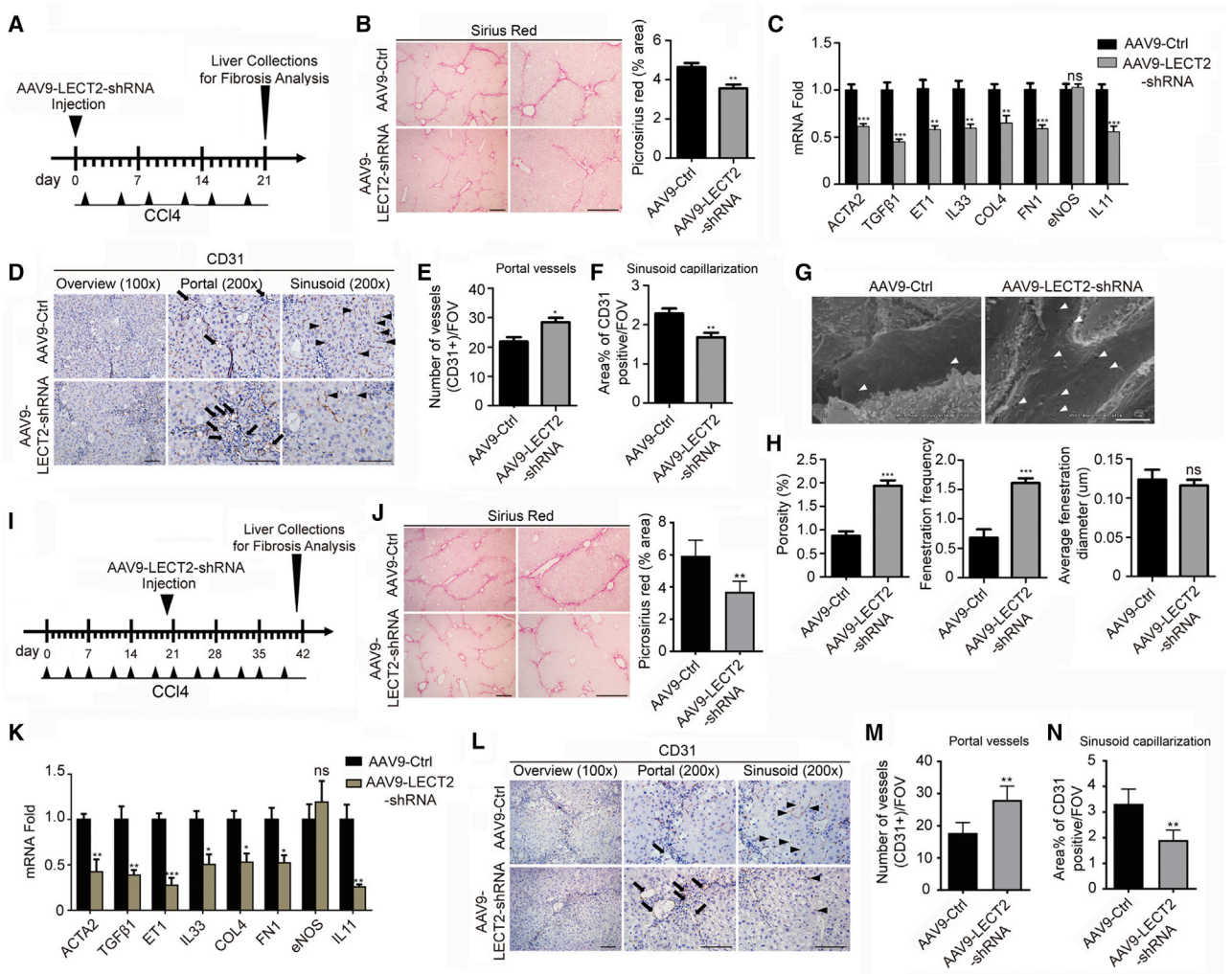

Figure 7. AAV9-LECT2-shRNA Decreases Liver Fibrosis

(A) Schematic overview of experimental design for (B)–(H).

(B) AAV9-LECT2-shRNA reduced liver fibrosis. Scale bar, 200 μm.

(C) Hepatic mRNA levels of fibrotic factors.

(D) Immunohistochemical staining of CD31 in liver tissues. Arrows, vessels; arrowhead, capillarization of liver sinusoids. Scale bar, 100 μm.

(E) The numbers of CD31+ vessels were counted under high magnification (200×).

(F) The capillarization of liver sinusoids were measured by digital image analysis of CD31 positivity under high magnification (200×).

(G) Scanning electron micrographs of the liver tissues from mice treated with CCl4 and AAV9-Ctrl (left) or mice treated with CCl4 and AAV9-LECT2-shRNA (right).

(H) Porosity (left), fenestration frequency (middle), and average fenestration diameter (right) were analyzed by ImageJ. Arrows, LSEC fenestrae. Scale bar, 2.5 μm.

(I) Schematic overview of experimental design for (J)–(N).

(J) AAV9-LECT2-shRNA infection reduced liver fibrosis.

(K) Hepatic mRNA levels of fibrotic factors.

(L) Immunohistochemical staining of CD31 in liver tissues. Arrows, vessels; arrowhead, capillarization of liver sinusoids. Scale bar, 100 μm.

(M) The numbers of $CD31^+$ vessels were counted under high magnification (200×).

(N) The capillarization of liver sinusoids were measured by digital image analysis of CD31 positivity under high magnification (200×). Mean ± SEM. *$p < 0.05$, **$p < 0.01$, ***$p < 0.001$.

See also Figure S7.

to Tie2/Tie2 homodimers. We clarified that LECT2 induces Tie1 dephosphorylation and Tie2 phosphorylation; activates MAPK/PPAR/MMP/VE-cadherin signaling pathway; inhibits EC migration and tube formation; inhibits portal angiogenesis; and induces sinusoid capillarization. All of these events lead to liver fibrogenesis (schematic in Figure S6F).

Tie1/Tie2 heterodimerization is critical for their downstream signal transmission (Saharinen et al., 2005; Seegar et al., 2010), and the Fn3 domain contributes to Tie1/Tie2 heterodimerization (Leppänen et al., 2017). It was reported that residues R260, R437, and R438 of Tie1 play a central role in receptor association with Tie2 (Seegar et al., 2010). Our study

showed that LECT2 bound to the Ig3 domain (aa360-436) of Tie1, and this domain is in the close vicinity of Fn domain and overlaps with the critical region of Tie1(R260, R437, and R438) for its interaction with Tie2. In this regard, it is not surprising that LECT2 can dissociate the interaction between Tie1 and Tie2.

Published literatures indicate that angiogenesis may contribute to the progression of fibrosis during the wound healing process in CLDs. Liver has two different types of microvascular structures: large vessels (such as portal vein, hepatic arteries) that are lined by a continuous ECs lying on a basement membrane, and liver sinusoids that are lined by fenestrated and discontinuous ECs. To the best of our knowledge, no previous studies have addressed the distinct roles of portal angiogenesis from sinusoids capillarization in liver fibrosis, and portal angiogenesis and sinusoid capillarization were often grouped together in hepatic angiogenesis studies. In the current study, we have provided robust data supporting a pro-fibrogenic role of LECT2. The key role of LECT2 in liver fibrogenesis was supported by our data derived from the *Lect2 KO* mice, where liver fibrosis of different etiologies including CCl4, BDL, DDC, and MCD was significantly attenuated. Attenuation of liver fibrosis in these models was accompanied by increased portal angiogenesis and decreased capillarization of the sinusoids. It is known that capillarization of the sinusoids results in a distorted structure of hepatic sinusoids and loss of specific endothelial fenestration. These changes decrease the permeability of sinusoids, and impair the physiological exchange of oxygen, nutrients, and metabolic factors between liver parenchyma and circulation system, resulting in hepatocyte damage and loss of functions. Meanwhile, insufficient portal vasculature can impair the entry of oxygen and nutrients into liver sinusoids, leading to worsened hepatocyte injury. Our studies suggest that portal angiogenesis and sinusoid capillarization play divergent roles during liver fibrogenesis: portal angiogenesis attenuates fibrogenesis, whereas sinusoid capillarization promotes fibrogenesis. It should be noted that, in studying angiogenesis in the liver, assessment of sinusoid capillarization by counting positively stained vascular markers (e.g., CD31) alone may "mask" the level of portal angiogenesis, leading to over-estimation of neovascularization. In our study, we observed that counting the CD31-positive portal vessels and sinusoid capillaries together could have led to a false conclusion of "increased angiogenesis." Hence, in our studies reported here, we defined sinusoid capillarization as vascular remodeling rather than angiogenesis, and these two functionally distinct processes were analyzed as two separate entities.

Anti-angiogenic treatments have even been found to prevent liver fibrosis (Elpek, 2015). However, no such therapies have yet been approved for clinical use in patients with liver fibrosis. Based on our data, inhibition of sinusoid capillarization by anti-angiogenenic therapies may prevent liver fibrosis, whereas inhibition of portal angiogenesis by anti-angiogenenic treatments may offset the efficiency of these treatments to prevent fibrogenesis. As such, we propose that a combinatorial use of promoting portal angiogenesis and simultaneous inhibition of sinusoid capillarization would help achieve better therapeutic effects for liver fibrosis. In this regard, LECT2-Tie1 signaling pathway may represent a valuable target for liver fibrosis treatment. This notion was very nicely validated in our studies reported here, in that knockdown of LECT2 by AAV9-LECT2 shRNA significantly attenuated liver fibrosis and inhibited sinusoid capillarization, while portal angiogenesis was markedly enhanced. Further support to this notion comes from our studies in *Lect2-KO* mouse model, where VEGF/VEGFR inhibitors sorafenib and bevacizumab were demonstrated to significantly attenuate liver fibrosis in *Lect2-KO* mice.

Our results have identified LECT2 as a functional ligand for orphan receptor Tie1 and provided valuable insights into a potential role of LECT2/Tie1 signaling in angiogenesis/sinusoid capillarization and liver fibrogenesis. Of clinical relevance, serum LECT2 level may serve as a potential diagnostic marker for liver fibrosis, and targeting LECT2/Tie1 signaling pathway may provide a new avenue for the treatment of this liver disease. Validation of our data in a large cohort of patients with liver fibrosis is certainly warranted.

STAR★METHODS

Detailed methods are provided in the online version of this paper and include the following:

- KEY RESOURCES TABLE
- LEAD CONTACT AND MATERIALS AVAILABILITY
- EXPERIMENTAL MODEL AND SUBJECT DETAILS
  - Patients and Clinical Specimens
  - Mice
  - Cell lines
- METHOD DETAILS
  - Fibrosis Models
  - Isolation of primary hepatocytes and non-parenchymal liver cells
  - Tube formation assay
  - Transwell migration assay
  - Immunohistochemistry
  - Immunofluorescence
  - Co-immunoprecipitation and western blot analysis
  - MBP pull-down assay
  - Plasmid construction and recombinant protein expression
  - qRT-PCR
  - ELISA assay
  - NanoBiT Protein:Protein interactions
  - Intrahepatic overexpression or knockdown of LECT2, Tie1, CD209a and VEGFR2
  - *in vitro* knockdown of LECT2, Tie1, Tie2, CD209a and VEGFR2
  - Scanning electron microscopy
  - Surface plasmon resonance (SPR) assay
  - Protein cross-linking coupled with mass spectrometry
  - Solid phase binding assay
  - Proteasome inhibitor and cycloheximide chase experiments
- QUANTIFICATION AND STATISTICAL ANALYSIS
  - Statistics
- DATA AND CODE AVAILABILITY

SUPPLEMENTAL INFORMATION

Supplemental Information can be found online at https://doi.org/10.1016/j.cell.2019.07.021.

ACKNOWLEDGMENTS

We thank Professor Jiong Chen of Ningbo University for providing the *Lect2-KO* mice. We thank Central Laboratory, Southern Medical University for providing facilities and technical support. This work was supported by the National Basic Research Program of China (973 program, 2015CB554002), the National Natural Science Foundation of China (81573015, 81600496, 31700114, 81773101, 31771578), Guangdong Provincial Natural Science Foundation for Distinguished Young Scientists (2015A030306048), Guangzhou Science and Technology Collaborative Innovation Major Projects (201704020071), Guangdong Key Research and Development Plan (2019B020234003), Frontier Research Program of Guangzhou Regenerative Medicine and Health Guangdong Laboratory (2018GZR110105002), Qilu Young Scholar of Shandong University (86963072), Natural Science Foundation of Jiangsu Province (BK20170399), and Project of the National Natural Science Foundation of China supported by NSFC-Guangdong Joint Fund (U1201226).

AUTHOR CONTRIBUTIONS

Conceptualization, W.-J.Z.; Methodology, M.X., H.-H.X., Y.L., X.S., L.-J.W., Z.-P.F., X.-H.S., X.-J.L., Y.H., Z.-M.L., Y.C., Y.W., J.L., L.L., H.-J.L., Z.C., N.T., C.P., T. Li, T. Liu, D.W., Y.-Q.D., and W.-J.Z.; Validation, M.X., H.-H.X., Y.L., X.S., X.-H.S., X.-J.L., Y.H., Z.-M.L., Y.C., C.P., D.W., and W.-J.Z.; Formal Analysis, M.X., H.-H.X., Y.L., X.S., L.Q., D.W., and W.-J.Z.; Investigation, M.X., H.-H.X., Y.L., X.S., L.-J.W., Z.-P.F., X.-H.S., X.-J.L., Y.H., Z.-M.L., C.P., D.W., and W.-J.Z.; Resources, L.-J.W., Z.-P.F., Y.C., Y.W., J.L., C.P., D.W., Y.-Q.D., and W.-J.Z.; Data Curation, M.X., H.-H.X., Y.L., X.S., D.W., and W.-J.Z.; Writing – Original Drafts, Y.L. and W.-J.Z.; Writing – Review & Editing, all authors; Visualization, M.X., H.-H.X., Y.L., X.S., D.W., and W.-J.Z.; Supervision, Y.L., D.W., and W.-J.Z.; Project Administration, Y.L. and W.-J.Z.; Funding Acquisition, L.-J.W., D.W., Y.-Q.D., and W.-J.Z.

DECLARATION OF INTERESTS

The authors declare no competing interests.

Received: February 14, 2018
Revised: April 23, 2019
Accepted: July 12, 2019
Published: August 29, 2019

REFERENCES

Augustin, H.G., Koh, G.Y., Thurston, G., and Alitalo, K. (2009). Control of vascular morphogenesis and homeostasis through the angiopoietin-Tie system. Nat. Rev. Mol. Cell Biol. *10*, 165–177.

Barton, W.A., Tzvetkova-Robev, D., Miranda, E.P., Kolev, M.V., Rajashankar, K.R., Himanen, J.P., and Nikolov, D.B. (2006). Crystal structures of the Tie2 receptor ectodomain and the angiopoietin-2-Tie2 complex. Nat. Struct. Mol. Biol. *13*, 524–532.

Berger, J., and Moller, D.E. (2002). The mechanisms of action of PPARs. Annu. Rev. Med. *53*, 409–435.

Chen, C.K., Yang, C.Y., Hua, K.T., Ho, M.C., Johansson, G., Jeng, Y.M., Chen, C.N., Chen, M.W., Lee, W.J., Su, J.L., et al. (2014). Leukocyte cell-derived chemotaxin 2 antagonizes MET receptor activation to suppress hepatocellular carcinoma vascular invasion by protein tyrosine phosphatase 1B recruitment. Hepatology *59*, 974–985.

Chen, C.K., Yu, W.H., Cheng, T.Y., Chen, M.W., Su, C.Y., Yang, Y.C., Kuo, T.C., Lin, M.T., Huang, Y.C., Hsiao, M., et al. (2016). Inhibition of VEGF165/VEGFR2-dependent signaling by LECT2 suppresses hepatocellular carcinoma angiogenesis. Sci. Rep. *6*, 31398.

Cogger, V.C., O'Reilly, J.N., Warren, A., and Le Couteur, D.G. (2015). A standardized method for the analysis of liver sinusoidal endothelial cells and their fenestrations by scanning electron microscopy. J. Vis. Exp. *30*, e52698.

Elpek, G.Ö. (2015). Angiogenesis and liver fibrosis. World J. Hepatol. *7*, 377–391.

Fujii, M., Inoki, I., Saga, M., Morikawa, N., Arakawa, K., Inaba, S., Yoshioka, K., Konoshita, T., and Miyamori, I. (2012). Aldosterone inhibits endothelial morphogenesis and angiogenesis through the downregulation of vascular endothelial growth factor receptor-2 expression subsequent to peroxisome proliferator-activated receptor gamma. J. Steroid Biochem. Mol. Biol. *129*, 145–152.

Gressner, A.M., and Weiskirchen, R. (2006). Modern pathogenetic concepts of liver fibrosis suggest stellate cells and TGF-beta as major players and therapeutic targets. J. Cell. Mol. Med. *10*, 76–99.

Huang, W., Eum, S.Y., András, I.E., Hennig, B., and Toborek, M. (2009). PPARalpha and PPARgamma attenuate HIV-induced dysregulation of tight junction proteins by modulations of matrix metalloproteinase and proteasome activities. FASEB J. *23*, 1596–1606.

Ichikawa, Y., Ishikawa, T., Momiyama, N., Kamiyama, M., Sakurada, H., Matsuyama, R., Hasegawa, S., Chishima, T., Hamaguchi, Y., Fujii, S., et al. (2006). Matrilysin (MMP-7) degrades VE-cadherin and accelerates accumulation of beta-catenin in the nucleus of human umbilical vein endothelial cells. Oncol. Rep. *15*, 311–315.

Ito, M., Nagata, K., Kato, Y., Oda, Y., Yamagoe, S., Suzuki, K., and Tanokura, M. (2003). Expression, oxidative refolding, and characterization of six-histidine-tagged recombinant human LECT2, a 16-kDa chemotactic protein with three disulfide bonds. Protein Expr. Purif. *27*, 272–278.

Kim, K.L., Shin, I.S., Kim, J.M., Choi, J.H., Byun, J., Jeon, E.S., Suh, W., and Kim, D.K. (2006). Interaction between Tie receptors modulates angiogenic activity of angiopoietin2 in endothelial progenitor cells. Cardiovasc. Res. *72*, 394–402.

Lan, F., Misu, H., Chikamoto, K., Takayama, H., Kikuchi, A., Mohri, K., Takata, N., Hayashi, H., Matsuzawa-Nagata, N., Takeshita, Y., et al. (2014). LECT2 functions as a hepatokine that links obesity to skeletal muscle insulin resistance. Diabetes *63*, 1649–1664.

Leppänen, V.M., Saharinen, P., and Alitalo, K. (2017). Structural basis of Tie2 activation and Tie2/Tie1 heterodimerization. Proc. Natl. Acad. Sci. USA *114*, 4376–4381.

Lim, Y.S., and Kim, W.R. (2008). The global impact of hepatic fibrosis and end-stage liver disease. Clin. Liver Dis. *12*, 733–746, vii.

Lin, Y., Fang, Z.P., Liu, H.J., Wang, L.J., Cheng, Z., Tang, N., Li, T., Liu, T., Han, H.X., Cao, G., et al. (2017). HGF/R-spondin1 rescues liver dysfunction through the induction of $Lgr5^{+}$ liver stem cells. Nat. Commun. *8*, 1175.

Lu, X.J., Chen, J., Yu, C.H., Shi, Y.H., He, Y.Q., Zhang, R.C., Huang, Z.A., Lv, J.N., Zhang, S., and Xu, L. (2013). LECT2 protects mice against bacterial sepsis by activating macrophages via the CD209a receptor. J. Exp. Med. *210*, 5–13.

Lu, S., Fan, S.B., Yang, B., Li, Y.X., Meng, J.M., Wu, L., Li, P., Zhang, K., Zhang, M.J., Fu, Y., et al. (2015). Mapping native disulfide bonds at a proteome scale. Nat. Methods *12*, 329–331.

Lu, X.J., Chen, Q., Rong, Y.J., Yang, G.J., Li, C.H., Xu, N.Y., Yu, C.H., Wang, H.Y., Zhang, S., Shi, Y.H., and Chen, J. (2016). LECT2 drives haematopoietic stem cell expansion and mobilization via regulating the macrophages and osteolineage cells. Nat. Commun. *7*, 12719.

Mereuta, O.M., Theis, J.D., Vrana, J.A., Law, M.E., Grogg, K.L., Dasari, S., Chandan, V.S., Wu, T.T., Jimenez-Zepeda, V.H., Fonseca, R., et al. (2014). Leukocyte cell-derived chemotaxin 2 (LECT2)-associated amyloidosis is a frequent cause of hepatic amyloidosis in the United States. Blood *123*, 1479–1482.

Ong, H.T., Tan, P.K., Wang, S.M., Hian Low, D.T., Ooi, L.L., and Hui, K.M. (2011). The tumor suppressor function of LECT2 in human hepatocellular carcinoma makes it a potential therapeutic target. Cancer Gene Ther. *18*, 399–406.

Partanen, J., Armstrong, E., Mäkelä, T.P., Korhonen, J., Sandberg, M., Renkonen, R., Knuutila, S., Huebner, K., and Alitalo, K. (1992). A novel endothelial cell

surface receptor tyrosine kinase with extracellular epidermal growth factor homology domains. Mol. Cell. Biol. *12*, 1698–1707.

Puri, M.C., Rossant, J., Alitalo, K., Bernstein, A., and Partanen, J. (1995). The receptor tyrosine kinase TIE is required for integrity and survival of vascular endothelial cells. EMBO J. *14*, 5884–5891.

Qu, X., Tompkins, K., Batts, L.E., Puri, M., and Baldwin, H.S. (2010). Abnormal embryonic lymphatic vessel development in Tie1 hypomorphic mice. Development *137*, 1285–1295.

Saharinen, P., Kerkelä, K., Ekman, N., Marron, M., Brindle, N., Lee, G.M., Augustin, H., Koh, G.Y., and Alitalo, K. (2005). Multiple angiopoietin recombinant proteins activate the Tie1 receptor tyrosine kinase and promote its interaction with Tie2. J. Cell Biol. *169*, 239–243.

Sato, T.N., Tozawa, Y., Deutsch, U., Wolburg-Buchholz, K., Fujiwara, Y., Gendron-Maguire, M., Gridley, T., Wolburg, H., Risau, W., and Qin, Y. (1995). Distinct roles of the receptor tyrosine kinases Tie-1 and Tie-2 in blood vessel formation. Nature *376*, 70–74.

Savant, S., La Porta, S., Budnik, A., Busch, K., Hu, J., Tisch, N., Korn, C., Valls, A.F., Benest, A.V., Terhardt, D., et al. (2015). The Orphan Receptor Tie1 Controls Angiogenesis and Vascular Remodeling by Differentially Regulating Tie2 in Tip and Stalk Cells. Cell Rep. *12*, 1761–1773.

Seegar, T.C., Eller, B., Tzvetkova-Robev, D., Kolev, M.V., Henderson, S.C., Nikolov, D.B., and Barton, W.A. (2010). Tie1-Tie2 interactions mediate functional differences between angiopoietin ligands. Mol. Cell *37*, 643–655.

Tsochatzis, E.A., Bosch, J., and Burroughs, A.K. (2014). Liver cirrhosis. Lancet *383*, 1749–1761.

Tyagi, N., Moshal, K.S., Sen, U., Lominadze, D., Ovechkin, A.V., and Tyagi, S.C. (2006). Ciglitazone ameliorates homocysteine-mediated mitochondrial translocation and matrix metalloproteinase-9 activation in endothelial cells by inducing peroxisome proliferator activated receptor-gamma activity. Cell. Mol. Biol. *52*, 21–27.

Yamagoe, S., Yamakawa, Y., Matsuo, Y., Minowada, J., Mizuno, S., and Suzuki, K. (1996). Purification and primary amino acid sequence of a novel neutrophil chemotactic factor LECT2. Immunol. Lett. *52*, 9–13.

Yoo, H.J., Hwang, S.Y., Choi, J.H., Lee, H.J., Chung, H.S., Seo, J.A., Kim, S.G., Kim, N.H., Baik, S.H., Choi, D.S., and Choi, K.M. (2017). Association of leukocyte cell-derived chemotaxin 2 (LECT2) with NAFLD, metabolic syndrome, and atherosclerosis. PLoS ONE *12*, e0174717.

Zhou, W.J., Geng, Z.H., Chi, S., Zhang, W., Niu, X.F., Lan, S.J., Ma, L., Yang, X., Wang, L.J., Ding, Y.Q., and Geng, J.G. (2011). Slit-Robo signaling induces malignant transformation through Hakai-mediated E-cadherin degradation during colorectal epithelial cell carcinogenesis. Cell Res. *21*, 609–626.

Zhou, W.J., Geng, Z.H., Spence, J.R., and Geng, J.G. (2013). Induction of intestinal stem cells by R-spondin 1 and Slit2 augments chemoradioprotection. Nature *501*, 107–111.

STAR★METHODS

KEY RESOURCES TABLE

REAGENT or RESOURCE	SOURCE	IDENTIFIER
Antibodies		
Rat monoclonal anti-CD31	Biolegend	Cat#102515; RRID:AB_2161030
Rat monoclonal anti-F4/80	Biolegend	Cat#123109; RRID:AB_893498
Mouse monoclonal anti-LECT2	Abcam	Cat#ab119429; RRID: AB_10899978
Rabbit monoclonal anti-LECT2	Abcam	Cat#ab196015
Mouse monoclonal anti-TIE1	Abcam	Cat#ab201986
Rabbit polyclonal anti-CD31	Abcam	Cat#ab28364; RRID: AB_726362
Chicken polyclonal anti-Albumin	Abcam	Cat#ab106582; RRID:AB_10888110
Mouse monoclonal anti-α-SMA	ShenDa	Cat#AM0005
Rat monoclonal anti-F4/80	Abcam	Cat#ab16911; RRID:AB_443548
Goat polyclonal anti-tdTomato	Biorbyt	Cat#orb182397; RRID:AB_2687917
Rabbit monoclonal anti-VEGFR2	Cell Signaling Technology	Cat#9698
Mouse monoclonal anti-CD11b/c	Abcam	Cat#ab1121
Mouse monoclonal anti-FLAG M2	Sigma-Aldrich	Cat#F1804; RRID: AB_262044
Mouse monoclonal anti-MYC-Tag	Proteintech	Cat#66004-1-Ig; CloneNo: 2D11A8
Mouse monoclonal anti-His-Tag	Proteintech	Cat#66005-1-Ig; RRID: AB_11232599
Rabbit polyclonal anti-TIE1	Invitrogen	Cat#PA527903; RRID:AB_2545379
Rabbit polyclonal anti-TIE1 (Phospho-Tyr1117)	Absci	Cat#AB12535
Goat polyclonal anti-Tie2	R&D	Cat#AF313; RRID:AB_355295
Rabbit polyclonal anti-Phospho-Tie-2 (Y992)	R&D	Cat#AF2720; RRID:AB_442172
Mouse monoclonal anti-p38	Abcam	Cat#ab31828; RRID:AB_881839
Rabbit polyclonal anti-p38(Phospho Y182)	Abcam	Cat#ab47363; RRID:AB_881848
Rabbit monoclonal anti-Met	Cell Signaling Technology	Cat#8198; RRID:AB_10858224
Rabbit monoclonal anti-Phospho-Met (Tyr1234/1235)	Cell Signaling Technology	Cat#3077; RRID:AB_2315156
Rabbit monoclonal anti- VEGFR2	Cell Signaling Technology	Cat#2479; RRID:AB_2212507
Rabbit monoclonal anti-Phospho-VEGFR2 (Tyr1175)	Cell Signaling Technology	Cat#2478; RRID:AB_331377
Rabbit polyclonal anti-VE Cadherin	Abcam	Cat#ab33168; RRID:AB_870662
Mouse monoclonal anti-α-Tubulin	Ray	Cat#RM2007; Lot: Z0305
Mouse monoclonal anti-Maltose Binding Protein (MBP)	Sigma-Aldrich	Cat#M6295; RRID:AB_260613
Bacterial and Virus Strains		
Mouse Lect2-shRNA AAV Virus	This paper	N/A
Mouse ctrl-shRNA AAV Virus	HanBio Co.,Ltd	Cat#HH20170615XAJ-AAV02
Human Lect2 overexpression lentivirus	This paper	N/A
Human ctrl overexpression lentivirus	Obio technology Co., Ltd.	Cat#H145
E.Coli BL21	Kangti Life Technology Co., Ltd.	Cat#KTSM104L;
E.Coli DH5α	Kangti Life Technology Co., Ltd.	Cat#KTSM101L
Biological Samples		
Healthy adults' liver tissue	Wenzhou Medical University	N/A
Patients' liver biopsies	Southern Medical University	N/A
Healthy adults and patients' serum	the First Affiliated Hospital of Anhui Medical University	N/A
Chemicals, Peptides, and Recombinant Proteins		
Carbon tetrachloride	Sigma-Aldrich	Cat#10000-0-AP; CAS: 56-23-5
Diethyl 1,4-dihydro-2,4,6-trimethyl-3, 5-pyridinedicarboxylate (DDC)	Sigma-Aldrich	Cat#137030; CAS: 632-93-9

(*Continued on next page*)

Continued

REAGENT or RESOURCE	SOURCE	IDENTIFIER
Human LECT2 Protein	Abcam	Cat#ab188467; Lot: GR3202526-2
Mouse VEGF164 Protein	Sino Biological	Cat#50159-MNAB
Golvatinib(E7050)	Selleck Chemicals	Cat#S2859; CAS: 928037-13-2
Vandetanib(ZD6474)	Selleck Chemicals	Cat#S1046; CAS: 443913-73-3
SB 203580	Sigma-Aldrich	Cat#M6191; CAS: 152121-47-6
GW9662	Sigma-Aldrich	Cat#S8307; CAS: 22978-25-2
Glutaraldehyde	Nacalai Tesque	Cat#170003-92; CAS: 111-30-8
Cycloheximide (CHX)	Sigma-Aldrich	Cat#C7698; CAS: 66-81-9
MBP beads	Sigma-Aldrich	Cat#A0512
Human collagen type IV	Chundubio	Cat#20180321
Heparin sodium	Solarbio	Cat#H8060; CAS: 9041-08-1
Chondroitin 4-sulfate	Solarbio	Cat#C9160; CAS: 9007-28-7
Hyaluronic acid	Solarbio	Cat#S7020; CAS: 9004-61-9
Fibrinogen	Solarbio	Cat#F8050; CAS: 9001-32-5
Human vitronectin	Solarbio	Cat#P00082
Critical Commercial Assays		
TruSeq RNA Sample Prep Kit	Illumina	Cat#RS-122-2001, RS-122-2002
Sanger sequencing	Sangon Biotech (Shanghai) Co., Ltd.	N/A
qRT-PCR	Stratagene	Cat#Mx3000P™
Experimental Models: Cell Lines		
Human: EA.hy926 Cells	ATCC	Cat#CRL-2922; RRID: CVCL_3901
Human: 293T	Shi Lab, the Department of Pathology, Southern Medical University	Professor Jian Shi
Experimental Models: Organisms/Strains		
Mouse: B6-Gt (Rosa26 Sor–TdTomato)	The Jackson Laboratory	Cat#JAX: 007905
Mouse: C57BL/6J-Lect2$^{em1(2A\text{-}cre)Smoc}$	This paper	N/A
Mouse: *Lect2-KO*	Chen Lab, the Ningbo University	Professor Jiong Chen; Lu et al., 2016
Oligonucleotides		
siRNA targeting sequence:LECT2 #1: 5′-GGCAAGTCTTCCAATGAGA-3′	This paper	N/A
siRNA targeting sequence:LECT2 #2: 5′-GGTGTTCGAATATCTGGAA-3′	This paper	N/A
siRNA targeting sequence: VEGFR2 #1: 5′-GGTAAAGATTGATGAAGAA-3′	This paper	N/A
siRNA targeting sequence: VEGFR2 #2: 5′-GGATGAACATTGTGAACGA-3′	This paper	N/A
shRNA targeting sequence:TIE1 #1: 5′-GCAACGGATCCTACTTCTA-3′	This paper	N/A
shRNA targeting sequence:TIE1 #2: 5′-GCCTCGAAACTGTGACGAT-3′	This paper	N/A
shRNA targeting sequence:TIE2 #1: 5′-CTGGGTTTATGGGAAGGACG-3′	This paper	N/A
shRNA targeting sequence:TIE2 #2: 5′- ATGACTGTGGACAAGGGAGA-3′	This paper	N/A
shRNA targeting sequence:CD209a #1: 5′- CATGAGGTGTCCTTAAATGG-3′	This paper	N/A

(*Continued on next page*)

Continued

REAGENT or RESOURCE	SOURCE	IDENTIFIER
shRNA targeting sequence:CD209a #2: 5′-CACATATTGCCATGTGCAAT-3′	This paper	N/A
shRNA targeting sequence:LECT2: 5′-GCTAACATAGCCAGCAAATCTT-3′	This paper	N/A
shRNA targeting sequence:control: 5′-TTCTCGAACGTGTCACGT-3′	Hanbio Biotechnology Co. Ltd	Cat#HH20170615XAJ-AAV02
Primers for plasmid construction, see Table S5	This paper	N/A
Primers for qRT-PCR, see Table S6	This paper	N/A
Primer s for *Lect2 KO* mice: F: 5′- CATAGCCAGGGGACTATGTTTTA- 3′; R: 5′- ATATAGTCATAGCTGCACACAGCA- 3′	This paper	Lu et al., 2016
Recombinant DNA		
pMKH-MBP-Tie1-Ig3 (expression vector for recombinant Tie1-Ig3)	This study	N/A
pIRES2-EGFP-Flag-Tie1 (expression vector for recombinant Tie1)	This study	N/A
pIRES2-EGFP-Flag-Tie1-E (expression vector for recombinant Tie1)	This study	N/A
pIRES2-EGFP-Flag-Tie1-C (expression vector for recombinant Tie1-E)	This study	N/A
pIRES2-EGFP-Flag-Tie1-EC (expression vector for recombinant Tie1-EC)	This study	N/A
pIRES2-EGFP-Flag-Tie1-EN (expression vector for recombinant Tie1-EN)	This study	N/A
pIRES2-EGFP-Flag-Tie1-EGF (expression vector for recombinant Tie1)	This study	N/A
pIRES2-EGFP-Flag-Tie1-Ig3 (expression vector for recombinant Tie1-Ig3)	This study	N/A
pIRES2-EGFP-Flag-Tie1-M1 (expression vector for recombinant Tie1-M1)	This study	N/A
pIRES2-EGFP-Flag-Tie1-M2 (expression vector for recombinant Tie1-M2)	This study	N/A
pIRES2-EGFP-Flag-Tie1-Ig3-M1 (expression vector for recombinant Tie1-M1)	This study	N/A
pIRES2-EGFP-Flag-Tie1-Ig3-M2 (expression vector for recombinant Tie1-M2)	This study	N/A
pIRES2-EGFP-Flag-Tie1-Ig3-M3 (expression vector for recombinant Tie1-M3)	This study	N/A
pIRES2-EGFP-Flag-Tie1-K870R (expression vector for recombinant Tie1-K870R)	This study	N/A
pIRES2-EGFP-Flag-Tie1-δIg3 (expression vector for recombinant Tie1-δIg3)	This study	N/A
pIRES2-EGFP-Myc-LECT2 (expression vector for recombinant LECT2)	This study	N/A
pIRES2-EGFP-Myc-LECT2-δ90-101 (expression vector for recombinant LECT2)	This study	N/A
pIRES2-EGFP-Flag -Tie2 (expression vector for recombinant LECT2)	This study	N/A
pBiT1.1-C-Tie1 (expression vector for recombinant Tie1)	This study	N/A
pBiT1.1-C-Tie2 (expression vector for recombinant Tie2)	This study	N/A

(*Continued on next page*)

Continued

REAGENT or RESOURCE	SOURCE	IDENTIFIER
pBit2.1-C-Tie1 (expression vector for recombinant Tie1)	This study	N/A
pBit2.1-C-Tie2 (expression vector for recombinant Tie2)	This study	N/A
Software and Algorithms		
ImageJ 1.51 s	N/A	https://imagej.nih.gov/ij/
GraphPad Prism6	N/A	https://www.graphpad.com/scientific-software/prism/
Biacore T100 Evaluation software	GE Health Sciences Inc.	https://www.gelifesciences.com/en/us/shop/protein-analysis/spr-label-free-analysis/software/getting-started-biacore-t100-p-05911
PLINK 2.0 alpha	Lu et al., 2015	https://www.cog-genomics.org/plink/2.0/

LEAD CONTACT AND MATERIALS AVAILABILITY

Further information and requests for resources and reagents should be directed to the Lead Contact, Weijie Zhou (weijiezhouum@163.com).

EXPERIMENTAL MODEL AND SUBJECT DETAILS

Patients and Clinical Specimens

The normal liver tissues (without fibrosis) were obtained from eight patients with cholecystolithiasis who underwent cholecystectomy in the Department of Hepatobiliary Surgery, Taizhou Hospital. The fibrotic liver tissues were obtained from 62 patients with histologically diagnosed liver fibrosis. Serum samples were obtained from healthy volunteers and cirrhotic patients of various Child-Pugh stages. Patient information is presented in Table S1 and Table S2. Informed written consents were obtained from all subjects. Subjects in our study were not involved in previous procedures and are drug or test naive. The study protocols concerning human subjects are consistent with the principles of the Declaration of Helsinki, and were approved by the Clinical Research Ethics Committee of Southern Medical University, Wenzhou Medical University, and the First Affiliated Hospital of Anhui Medical University.

Mice

B6-Gt (Rosa26 Sor–TdTomato) mice were obtained from Beijing Vitalstar Biotechnology Co. Ltd (Beijing, China). *Lect2-cre* transgenic mice were obtained from Shanghai Model Organisms Center (Shanghai, China). *Lect2-Cre/Rosa26-Tomato* mice were generated by crossing *Lect2-cre* transgenic mice with Rosa26 Sor–TdTomato) mice. *Lect2-KO* mice were provided by Professor Jiong Chen of the Ningbo University with genotyping confirmation as previously reported (Lu et al., 2016). Briefly, genomic DNA was extracted from the *Lect2 KO* mice and PCR amplified using the forward (F) and reverse (R) primers (F: 5‘- CATAGCCAGGGGACT ATGTTTTA- 3‘, R: 5‘- ATATAGTCATAGCTGCACACAGCA- 3‘). The product of 377 bp was used for the amplicon with its sequence confirmed by Sanger sequencing. C57BL/6 mice were purchased from the Guangdong Medical Laboratory Animal Centre (Guangzhou, China). All studies were performed in male mice unless otherwise indicated. Mice were kept in a standard 12 h light–dark cycle under the specific-pathogen–free conditions, and were allowed for free access to water and food. All the mice we used were healthy and immune-normal. Animal related research protocols are consistent with the U.S. Public Health Service Policy on Use of Laboratory Animals, and were approved by the Ethics Committee on Use and Care of Animals of Southern Medical University.

Cell lines

EA.hy926 Cells (ATCC Number: CRL-2922, RRID:CVCL_3901) were obtained from the American Type Culture Collection (ATCC) and generated in the Department of Pathology, Nanfang Hospital. 293T cells were kindly provided by Professor Jian Shi of the Southern Medical University. Both EA.hy926 cells and 293T cells were cultured in DMEM (GIBCO) full medium with 10% FBS at 37°C in a humidified atmosphere of 5% CO_2. The cell lines have been identified to be correct.

METHOD DETAILS

Fibrosis Models

To induce chronic liver fibrosis, 6-week old male mice were injected with CCl4 (Sigma-Aldrich, 2 ml/kg, in olive oil at a ratio of 1:4, i.p., twice a week for 10 weeks). Animals were sacrificed 24 h after the last injection of CCl4. Serum samples were collected and the liver tissues were harvested for subsequent analyses.

For BDL model, the common bile duct was doubly ligated with 4–0 silk and transected between the ligated sites. Sham-operated mouse were operated on similarly as control of C57BL/6 mice, except the bile duct was not ligated or transected. Liver tissues and serum samples were collected 3 weeks after the operation.

For 3,5-diethoxycarbonyl-1,4-dihydrocollidine (DDC) diet–induced cholestatic liver injury, 6-week old male mice were fed a diet containing 0.1% DDC (Sigma-Aldrich 137030-25G) for 8 weeks. The liver tissues and serum samples were collected for analysis.

For the methionine choline deficient (MCD) diet-fed mice model, 6-week-old male mice were fed MCD diet or control methionine choline sufficient (MCS) diet for six weeks. The liver tissues and serum samples were collected for analysis.

Sorafenib (Selleck, S7397) and Bevacizumab (Selleck, A2006) were used to suppress angiogenesis and VEGF/VEGFR2 signaling pathway. 6-week old male mice were injected i.p. with CCL4 for hepatic fibrosis as described before. Sorafenib was given every day by oral administration (50mgkg^{-1}) and Bevacizumab was given through tail vein twice a week (2mgkg^{-1} at the first week, and 1mgkg^{-1} at the rest of time) during hepatic fibrosis process. The liver samples were collected after 3 weeks.

For Sirius Red staining, 2.5-μm sections were stained with Sirius Red (LEAGENE, DC0041) and results were quantified using Nikon Elements software. Six random fields from each section were analyzed under the magnification of 100 ×, Five random sections from each mouse were analyzed and data from 5-10 mice per group were used in the comparison between different treatment groups.

Isolation of primary hepatocytes and non-parenchymal liver cells

A two-step collagenase perfusion procedure was used to isolate mouse hepatocytes as previously reported with slight modifications. Mice (male, 6 weeks-old) were perfused through portal vein cannulation by Hank's balanced salt solution (HBSS) (GIBCO, 14175500BT) containing 15 mM HEPES (GIBCO, 15630080) and 1% penicillin-streptomycin (GIBCO, 15140163) (Step 1), followed by the enzymatic solution DMEM (GIBCO, 11995500BT) containing 15 mM HEPES, 1% penicillin-streptomycin and 90 u/ml collagenase IV (Thermo Fisher Scientific, 17104019) (Step 2). The cell suspensions were filtered through a 70 μm nylon mesh, centrifuged at 50 g for 5 min at 4°C, and the cell pellets (hepatocytes) were collected. The supernatants were further centrifuged at 200 x g for 10 min at 4°C to obtain LESCs, ECs and KCs, and at 580 x g for 10 min at 4°C to obtain HSCs.

HSCs, ECs and KCs were further sorted using flow cytometry. For FACS-based purification of HSCs, endogenous retinoid fluorescence was used as a selection marker and was measured by the same setting as is for DAPI (excitation wavelength of 405–407 nm and detection wavelength of 450-500 nm. ECs and KCs were identified by staining with antibodies for mouse CD31 (Biolegend, 102515) and F4/80 (Biolegend, 123109), respectively. Isolation of LSECs and KCs were performed through a density gradient of 50% and 25% Percoll (GE Healthcare, 17-0891-09). The LSECs were separated from the KCs from the gradient interphase layer by selective adhesion on standard Petri dishes and cultured in DMEM supplemented with 10% FBS, 1% penicillin streptomycin (GIBCO) and 10 nM VEGF (Sino Biological, 50159-MNAB) at 37°C in a humidified atmosphere of 5% CO_2.

Tube formation assay

Tube formation assay is a well-established *in vitro* method for assessing the abilities of cells to form capillary-like tube structures as an indication for angiogenesis. Formation of capillary-like tubes on Matrigel requires cell-matrix interaction and cellular communication and motility. To examine the effect of LECT2 on angiogenesis *in vitro*, EA.hy926 cells or primary LSECs were seeded in 24-well culture plates (6 × 10^4 cells/well) precoated with Matrigel. Cells were treated with 5 nM of recombinant human LECT2 (rLECT2) (Abcam, ab188467) for 6 h. Primary LSEC were cultured for two weeks before being seeded in μ–Slide Angiogenesis kit (ibidi, Germany) at a density of 3.5 × 10^4 cells/well. Cells were then treated with 5 nM of rLECT2 for four hours. Tube formation was visualized under an inverted microscope, and the numbers and lengths of the tubes were measured in five randomly chosen fields under the microscope. To examine whether LECT2 regulate the tube forming ability of EA.hy926 cells through Tie1, stable EA.hy926 cells with Tie1 knockdown were generated by transfecting the cells with Lenti-Tie1-shRNAs or Lenti-Ctrl-shRNA. These stables cells and their controls were transfected with VEGFR2-siRNAs for 72 h, or were treated with 5 μM of Golvatinib (an inhibitors for Met and VEGFR2) or the same dose of Vandetanib (an inhibitor for VEGFR2) (both from Selleckchem for 6 h in the presence or absence of 5 nM rLECT2.

Transwell migration assay

For cell migration assay, EA.hy926 cells (1 × 10^5) were seeded into the upper chambers of 24-well transwell plate (Corning, Costar 3422). Fetal calf serum (10%) was added to the lower chamber. For the migration assay in primary LSECs, 2.4 × 10^5 cells were seeded into the upper chambers with 2% FBS. The lower chamber contains 20% FBS. These cells were maintained in culture conditions at 37°C in the presence or absence of 5 nM of rLECT2, and allowed to migrate for 6 h (for EA.hy926 cells) or 36 h (for primary LSECs). Unmigrated cells in the upper chamber were wiped with a cotton tip. The migrated cells on the underside of the filter were fixed, stained with hematoxylin, and counted in five randomly chosen fields per insert. To examine whether LECT2 regulates the migration of EA.hy926 cells through Tie1, EA.hy926 cells were transfected with Tie1-siRNAs, VEGFR2-siRNAs, or c-Met-siRNAs for 72 h, or treated with 5 μM of Golvatinib or the same dose of Vandetanib for 6 h in the presence or absence of 5 nM rLECT2.

Immunohistochemistry

Human liver biopsies (0.5-1 cm^3) were fixed in 10% neutral buffered formalin, dehydrated and embedded in paraffin, as we previously reported (Zhou et al., 2011, 2013; Lin et al., 2017). Sections of 2.5-μm thickness were incubated in citrate buffer (pH 6.0) for 5 min at 120°C, and the endogenous peroxidase was blocked by 0.3% H_2O_2 for 10 min. The slides were incubated with 5% BSA in PBS for

30 min at 37°C to block the non-specific binding sites, followed by incubation with appropriate primary antibodies for overnight at 4°C, and then with horseradish peroxidase (HRP) anti-rabbit IgG or anti-mouse IgG antibodies for 1 h. Color was then developed by incubation with DAB Substrate kit (Zsbio, ZLI-9017). After washing in PBS, tissue sections were counterstained with hematoxylin and viewed under a microscope. Major primary antibodies used in the study include anti-human LECT2 antibody (1:150, ab119429, RRID:AB_10899978), anti-mouse LECT2 antibody (1:700, Abcam, ab196015), anti-Tie1 antibody (1:200, Abcam, ab201986), and anti-CD31 antibody (1:50, Abcam, ab28364, RRID:AB_726362).

In Figures 3 and 6, vessels were manually counted based on immunohistochemistry staining of CD31. Five randomly chosen fields from each section were analyzed at the magnification of 200 ×.

Immunofluorescence

Immunofluorescent staining of liver tissues was performed as we reported (Zhou et al., 2011, 2013; Lin et al., 2017). Briefly, liver tissues were fixed with 10% neutral buffered formalin, cut into sections of 2.5-μm thickness, incubated with citrate buffer (pH 6.0) for 4 min at 100% power and for additional 15 min at 20% power in microwave. After the non-specific binding sites were blocked with goat serum for 10 min at 37°C, the sections were incubated with appropriate primary antibodies at 37°C overnight, washed extensively in PBS, with Alexa488/594 conjugated secondary antibodies (Cytoskeleton Inc., Denver, USA) for 1 h. Sections were then counterstained with 4, 6-diamidino-2-phenylindole (DAPI), washed and mounted for observation under a scanning confocal microscope (Olympus, Fluoview FV1000). The following primary antibodies were used for immunofluorescence: Anti-LECT2 antibody (1:3500, Abcam, ab196015), anti-Tie1 antibody (1:1000, Abcam, ab201986), anti-CD31 antibody (1:250, Abcam, ab28364), anti-ALB antibody (1:1000, Abcam, ab106582), anti-α-SMA antibody (1:500, ShenDa GuangZhou, AM0005), anti-F4/80 antibody (1:500, Abcam, ab16911), anti-tdTomato antibody (1:2500, Biorbyt, orb182397). anti-VEGFR2 antibody (1:1000, Cell Signaling Technology, 2479), and anti-CD11b antibody (1:500, Abcam, ab1211).

Co-immunoprecipitation and western blot analysis

For co-immunoprecipitation (Co-IP), 10^6 cells were lysed using 1 mL of lysis buffer (Tris-HCL 50mM, PH 7.4, Nacl 150 mM, sodium deoxycholate 0.25%, NP-40 1%, EDTA 1 mM, PMSF 1 mM, Aprotinin 1 μg/ml, leupeptin 1 μg/ml, pepstain 1 μg/ml) on ice for 30 min, and centrifuged at 12,000 rpm for 15 min. The supernatant was incubated with appropriate primary antibodies overnight, followed by incubating with protein A/G PLUS-Agarose beads (Santa Cruz Biotech., sc-2003) for 4 h. After washing for three times using ice-cold lysis buffer, beads were boiled with 5x loading buffer for 5 min followed by SDS-PAGE and western blotting using the appropriate primary and second antibodies. The protein bands were visualized using enhanced chemiluminescence detection system (Amersham Biosciences Europe, Freiberg, Germany) according to the manufacturer's instructions.

For amplify the plasmids for wild-type Myc-tagged LECT2, Flag-tagged Tie1 and Flag-tagged Tie1 truncations, 293T cells were transiently transfected with the appropriate constructs. After 48 h, cells were lysed in radioimmunoprecipitation assay (RIPA) buffer in the presence of complete protease inhibitors.

To investigate the interactions between PPARγ or MAPK pathways and LECT2 on endothelial cells, EA.hy926 cells were treated with 5 nM of rLECT2 in the presence or absence of GW9662 or SB203580 (both from Sigma-Aldrich) for 24 h. The expression of VE-cadherin in the cell lysates was examined by immunoblotting using anti-VE-cadherin antibody.

The following primary antibodies were used for co-immunoprecipitation and western blotting: Anti-Flag antibody (1:1000, Sigma-Aldrich, F1804, RRID:AB_262044), anti-MYC antibody (1:1000, Proteintech, 66004-1-Ig), anti-His antibody (1:1000, proteintech, 66005-1-Ig, RRID:AB_11232599), anti-LECT2 antibody (1:1000, Abcam, ab196015), anti-Tie1 antibody (1:500, Invitrogen, PA5-27903, RRID:AB_2545379), anti-Tie1Phospho-Tyr1117 antibody (1:500, Abcam, AB12535), anti-Tie2 antibody (1 μg/ml, R&D, AF313, RRID:AB_355295), anti-Tie2-Phospho-Y992 antibody (0.5 μg/ml, R&D, AF2720, RRID:AB_442172), anti-p38 antibody (1:1000, Abcam, ab31828), anti-PhosphoY182-p38 antibody (1:2000, Abcam, ab47363) anti-Met antibody (1:1000, Cell Signaling Technology, 8198, RRID:AB_10858224), anti-Met-Phospho-Tyr1234/1235 antibody (1:1000, Cell Signaling Technology, 3077, RRID:AB_2315156), anti-VEGFR2 antibody (1:1000, Cell Signaling Technology, 2479, RRID:AB_2212507), anti-VEGFR2-Phospho-Tyr1175 antibody (1:1000, Cell Signaling Technology, 2478, RRID:AB_331377), anti-VE-cadherin (1:2000, Abcam, ab33168), and anti-α-Tubulin antibody (1:1000, Beijing Ray Antibody Biotech, RM2007). For western blotting, the following secondary antibodies were used: goat anti-Mouse IgG HCS (1:10000, Abbkine, A25112), goat anti-Mouse IgG LCS (1:10000, Abbkine, A25012), goat anti-Mouse IgG (1:5000, Boster, BA1050), goat anti-Rabbit IgG (1:5000, Boster, BA1054), and rabbit anti-Goat IgG (1:5000, Boster, BA1060).

MBP pull-down assay

His-tagged LECT2 proteins (rLECT2) were purchased from Abcam (ab188467), The recombinant plasmids pMKH-MBP-hTie1-Ig3 and pMKH-MBP were transformed into *E. coli* (BL21), respectively. *E. coli* pellets were collected after IPTG-induced overnight expression and lysed by sonication. Supernatant samples after centrifugation were used in the subsequent two-step purification by His•Bind resin and gel-filtration. For MBP pull-down assay, 3 μg of purified MBP or MBP-Tie1-Ig3 and 3 μg of rLECT2 were incubated with 20 μL MBP beads (Sigma-Aldrich, A0512) for 2 h in PBS at 4°C. After extensive washing, samples were suspended in the reducing SDS loading buffer, boiled for 5 min, and subjected to SDS-PAGE followed by immunoblotting. The primary antibodies used include anti-MBP (1:1000, Sigma-Aldrich, M6295) and His tag (1:500, Proteintech, 66005-1-1g, RRID:AB_11232599).

Plasmid construction and recombinant protein expression

The full-length myc-tagged human LECT2 cDNA and flag-tagged human Tie1 cDNA were purchased from Obio technology Co. Ltd. (Shanghai, China). The full-length flag-tagged human Tie2 cDNA was purchased from Genechem Co. Ltd. Using the plasmid of wild-type human Tie1 as the template, Tie1 encoding extracellular domain (Tie1-E, aa1-759); Tie1 encoding cytoplasmic domain (Tie1-C, aa785-1138); Tie1 encoding C-terminal extracellular domain (Tie1-EC, aa437-759), Tie1 encoding N-terminal extracellular domain (Tie1-EN, aa1-436), Tie1 encoding extracellular Ig1 and Ig2 domains (Tie1-Ig12, aa1-160), Tie1 encoding three extracellular EGF like domains (Tie1-EGF, aa160-360), Tie1 encoding extracellular Ig3 domain (Tie1-Ig3, aa360-436), Tie1 encoding extracellular aa68-aa377 (Tie1-M1), Tie1 encoding extracellular aa378-aa666 (Tie1-M2), Tie1 Ig3 deletion (Tie1-δIg3), Tie1 encoding extracellular Ig3 domain with mutations of L360I, F362V (Tie1-Ig3-M1), Tie1 encoding extracellular Ig3 domain with mutations of L364S, E365G, T366K, M367F, P368N, and R369P (Tie1-Ig3-M2), Tie1 encoding extracellular Ig3 domain with mutations of A373K, A375S, and N377W (Tie1-Ig3-M3), and kinase dead Tie1 (Tie1K870R) were constructed into H340 pIRES2-EGFP-3Flag vector, fused with flag tags for mammalian expression. For recombinant human extracellular Ig3 domain of Tie1 fused with MBP (MBP-Tie1-Ig3), Tie1 encoding extracellular Ig3 domain (aa360-436) was constructed into the pMKH vector for MBP-fusion proteins. LECT2 with aa90-aa101 deletion was constructed into the pires2-egfp vector, fused with myc tags for mammalian expression. All constructs were verified by DNA sequencing analysis. rTie1-Ig3 was expressed by *E.Coli* BL21 and purified using glutathione Sepharose beads (Sigma). MBP-Tie1-Ig3 was expressed by *E.Coli* BL21 and purified using MBP beads (Sigma). Sequences of the primers used for plasmid construction are listed in Key Resources Table.

qRT-PCR

Total RNA from human patient samples, mouse livers, and cell lines were extracted using the Trizol reagent, and reverse transcribed using Takara PrimeScript^{TM} RT Master Mix. The resulting cDNAs were used for PCR using the SYBR-Green Master PCR Mix (Applied Biosystem). All PCR reactions were conducted in the Mx3000 qPCR System (Stratagene, Mx3000P^{TM}) in triplicates. All data were normalized against endogenous GAPDH controls of each smaple. The relative quantitation value for each target gene compared to the calibrator for that target is expressed as $2^{-(Ct-Cc)}$ (where Ct and Cc are the mean threshold cycle differences after normalizing to GAPDH). Primers for qPCR were designed using NCBI Primer-BLAST and are listed in Key Resources Table.

ELISA assay

To measure serum levels of LECT2, ALT and AST, serums were collected from Human patients or mice. The serum levels of LECT2, ALT and AST in patients and mice were measured by ELISA. The assay kits for human LECT2 (Cat No: SEF541Hu), mouse LECT2 (Cat No: SEF541Mu), mouse ALT (Cat No: SEA207Mu) and mouse AST (Cat No: SEB214Mu) were purchased from Wuhan USCN Business Co. (Wuhan, China).

NanoBiT Protein:Protein interactions

The NanoBiT Protein:Protein interactions system was purchased from Promega (N2014). Full length cDNAs for Tie1 and Tie2 were amplified and constructed into the pBiT1.1-C [TK/LgBit] vector and pBit2.1-C [TK/SmBit] vector, using the plasmid of wild-type human Tie1 or Tie2 as the templates, respectively. LECT2-siRNA was used to knock down LECT2 in 293T cells. Tie1/pBiT1.1-C together with Tie2/pBiT2.1-C were transfected into LECT2 knockdown 293T cells for Tie1-Tie2 interaction measurement. Tie1/pBiT1.1-C and Tie1/pBiT2.1-C were simultaneously transfected into LECT2 knockdown 293T cells for Tie1-Tie1 interaction measurement Tie2/pBiT1.1-C and Tie2/pBiT2.1-C were simultaneously transfected into LECT2 knockdown 293T cells for Tie2-Tie2 interaction measurement. After 48 h of transfections, cells were incubated with 5 nM of rLECT2 for 30 min before the luminescent signals were measured.

Intrahepatic overexpression or knockdown of LECT2, Tie1, CD209a and VEGFR2

The custom-made lentivirus with full-length cDNA of human LECT2 was purchased from Obio technology Co. Ltd. (Shanghai, China). pLenti-EF1a-EGFP-P2A-Puro-CMV-Lect2-3Flag mock vectors was used as controls. These lentiviral vectors were injected into mice (1×10^8 TU, via tail vein) to overexpress LECT2.

The custom-made adenoviral vector carrying shRNA for mouse Tie1 (Ad-Tie1-shRNA), shRNA for mouse CD209a (Ad-CD209a-shRNA), shRNA for mouse VEGFR2 (Ad-VEGFR2-shRNA), and mouse nonsense control shRNA (Ad-Ctrl shRNA) were purchased from Hanbio Biotechnology Co. Ltd. (Shanghai, China). The adenovirus were injected into mice (1×10^8 pfu, via tail vein) to knock down Tie1, CD209a and VEGFR2, respectively. Target sequences are listed in Key Resources Table.

in vitro knockdown of LECT2, Tie1, Tie2, CD209a and VEGFR2

For *in vitro* knockdown of LECT2, Tie1, Tie2, CD209a and VEGFR2 in EA.hy926 cells, siRNAs of human LECT2, Tie1, CD209a, VEGFR2 and control nonsense siRNA were transfected into EA.hy926 cells. siRNAs were purchased from Guangzhou Ribobio Co., Ltd. (Guangzhou, China). For LECT2 overexpression, the custom-made lentiviral vector with human LECT2 cDNAs and the same for human control cDNAs were purchased from Obio technology Co. Ltd. (Shanghai, China). These lentiviral vectors were added to the culture media at a concentration of 1×10^8 TU. Target sequences are listed in Key Resources Table.

Scanning electron microscopy

The scanning electron microscopy was performed as reported (Cogger et al., 2015). Perfusion fixation of the mouse liver was performed with the mice under general anesthesia with 2.5% glutaraldehyde (Nacalai Tesque 17003-92). Images were obtained using Hitachi S-3000N scanning electron microscope. The average fenestration diameter, porosity (%) and fenestration frequency of the liver sinusoids were calculated in four random fields from each section at approximately 10,000 × magnification using ImageJ software. Average fenestration diameter was calculated as the average of all fenestration diameters (excluding gaps if they are $\geq$ 250 nm). Porosity was calculated by the equation: Porosity (%) = (Σ (πr^2)/total area analyzed - Σ (area of gaps, μm^2)) × 100. Fenestration frequency was calculated by the formula: fenestration frequency = total number of fenestrations/(total area analyzed- Σ(area of gaps, μm^2).

Surface plasmon resonance (SPR) assay

All SPR measurements were carried out on a Biacore T100 instrument (GE Health Sciences Inc.). The standard running buffer contained 20 mM HEPES (pH 8.0), 150 mM NaCl, and 0.005% Tween 20. All solutions were sterilized by filtering through 0.22 μm pore-sized filters and degassed at room temperature. Flow cells of the SPR CM5 chip were activated using N-hydroxy succinimide (NHS) and 1-ethyl-3-(3-dimethylaminopropyl) carbodiimide (EDC) for 7 min at a flow rate of 20 μL/min. For LECT2 immobilization, a solution of LECT2 protein at 40 μM in 10 mM sodium acetate (pH 5.0) was passed over one flow cell until > 100 response units (RU) were achieved. Activated free binding sites on the chip were blocked using 1M ethanolamine for an additional 7 min. All experiments were carried out at 25°C at a 30 μL/min flow rate and 120 s contact time, followed by a dissociation of 600 s and a regeneration injection of glycine for 60 s at pH 1.5. Kinetic curve fittings and K_d value calculations were performed with a 1:1 binding model using the Biacore T100 Evaluation software (GE Health Sciences Inc.).

Protein cross-linking coupled with mass spectrometry

MBP-Tie1-Ig3 and LECT2 (both at 100 uM, in 20 mM HEPES, pH 8.0) were added into the reaction solution at a ratio of 1:1. Bis (sulfosuccinimidyl) substrate (BS3, 2 mg, no-weigh format, Thermo Fisher Scientific) was freshly dissolved into HEPES buffer and immediately added to the MBP-Ig3 and LECT2 complex at a final concentration of 0.1-0.8 mM. The cross-linking reaction proceeded for 3 hr on ice and was quenched by 1 M Tris HCl (pH 7.5) at the final concentration of 50 mM. The quenching reaction was incubated at room temperature for 15 minutes. MBP-Tie1-Ig3 and LECT2 were incubated with BS3 (15-fold molar excess) for 1 hr. Reaction was quenched with 50 mM Tris buffer. The proteins were precipitated and digested for 16 hr at 37°C by trypsin at an enzyme-to-substrate ratio of 1:50 (w/w). The digested peptides were desalted and loaded on an in-house packed capillary reverse-phase C18 column (40 cm length, 100 μM ID x 360 μM OD, 1.9 uM particle size, 120 Å pore diameter) connected to an Easy LC 1200 system. The samples were analyzed with a 120 min-HPLC gradient from 6% to 35% of buffer B (buffer A: 0.1% formic acid in Water; buffer B: 0.1% formic acid in 80% acetonitrile) at 300 nL/min. The eluted peptides were ionized and directly introduced into a Q-Exactive mass spectrometer using a nano-spray source. Survey full-scan MS spectra (from m/z 300–1800) were acquired in the Orbitrap analyzer with resolution r = 70,000 at m/z 400. Cross-linked peptides were identified and evaluated using pLink2 software as described previously (Lu et al., 2015).

Solid phase binding assay

Different ECM components, including collagen type IV (20 μg/ml, Chundubio), heparin sodium (200 μg/ml, Solarbio), chondroitin sulfate (200 μg/ml, Solarbio), hyaluronic acid (200 μg/ml, Solarbio), matrigel (10 mg/ml, BD), fibrinogen (10 μg/ml, Solarbio), and vitronectin (20 μg/ml, Solarbio), were used to coat the 96-well enzyme-linked immunosorbent assay (ELISA) plates for overnight at 4°C. The coated plates were washed and blocked with 0.5% bovine serum albumin, incubated with rLECT2 (100 ng/ml) for overnight at 4°C. After extensive washing, the bound rLECT2 were detected. The binding affinity of rLECT2 to different ECM components was determined in the solid phase binding assays, which revealed that rLECT2 has a strong affinity to fibrinogen, a moderate affinity to Matrigel, but no affinity to collagen type IV, heparin sodium, chondroitin sulfate, hyaluronic acid, and vitronectin. All the experiments were performed in triplicates.

Proteasome inhibitor and cycloheximide chase experiments

For proteasome inhibitor assay, 5 nM of rLECT2 with or without proteasome inhibitor MG-132 (5 μM) were added into culture medium of EA.hy926 cells. After 1 hr, cells were harvested, and the protein expression level of Tie2 was measured by western blotting using anti-Tie2 antibody. For CHX chase assay, EA.hy926 cells were cultured in 6-well plates (10^6 cells/well) for 48 hr. Cells were then treated with 100 μg/ml of actinomycin (CHX) with or without 5 nM of rLECT2 for 0, 0.5, 1 and 2 hr, respectively. Cell lysates were collected to measure Tie2 protein level by western blotting.

QUANTIFICATION AND STATISTICAL ANALYSIS

Statistics

The experimental data were statistically analyzed by Student's t test or paired t test. All data are presented as mean ± s.e.m. A $p < 0.05$ was considered statistically significant. In all cases, data from at least three independent experiments was used. All

calculations were performed using SPSS software package. No randomization was used. No blinding was done. Power calculations were not done to predetermine sample sizes.

DATA AND CODE AVAILABILITY

All original data and RNaseq data are available at Mendeley dataset:
https://data.mendeley.com/datasets/fm63mc6hyv/draft?a=1d393817-1e36-4018-9285-a39ae92d5254

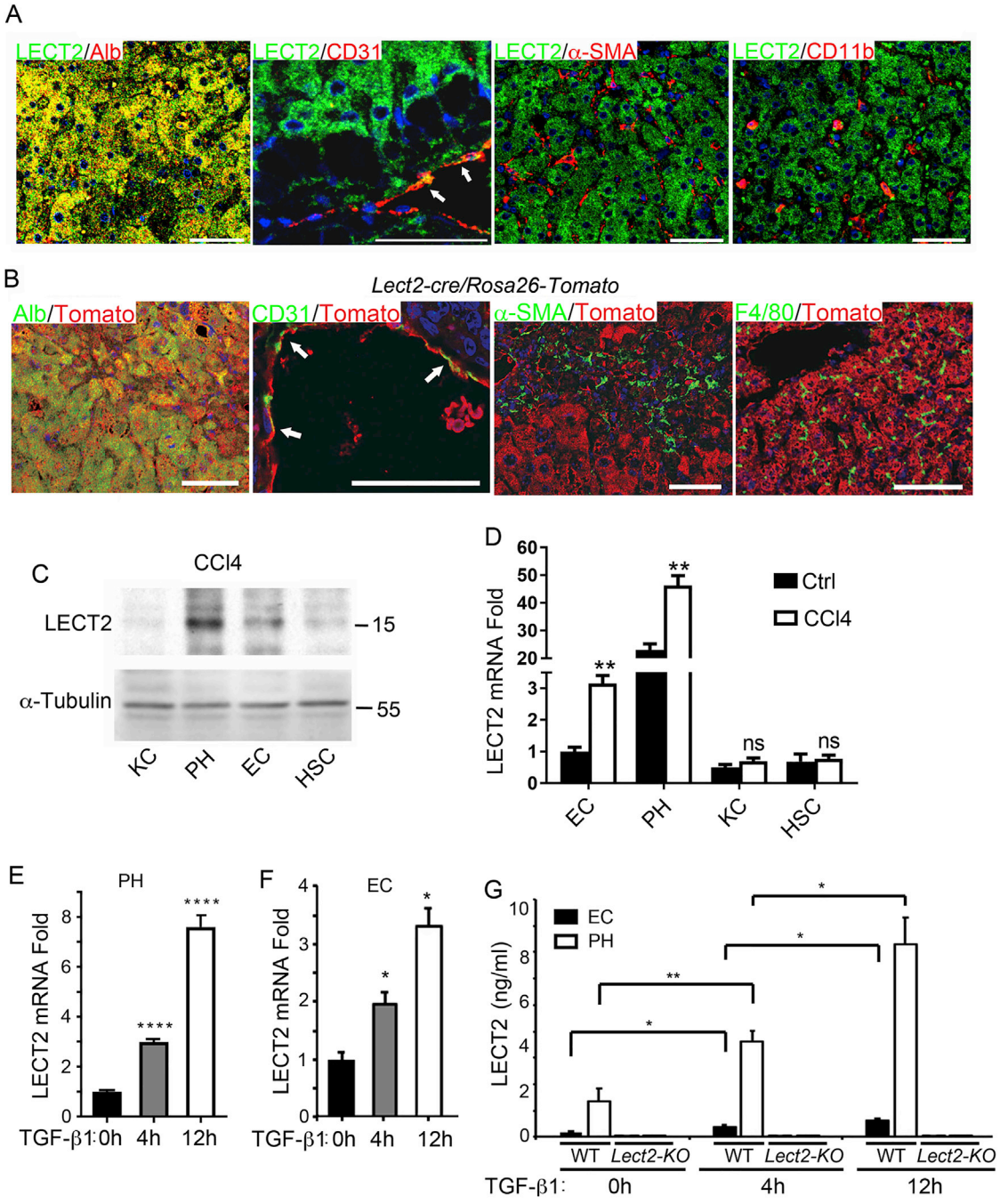

Figure S1. The Cellular Source of LECT2, Related to Figure 1

A, Human liver cirrhosis samples were processed for immunofluorescence co-staining for LECT2 with Alb (hepatocyte marker), CD31 (endothelial marker), α-SMA (activated HSC marker), and CD11b (macrophage marker). Slides were counterstained with DAPI. Arrows, ECs. Scale bar, 20 μm. B, *Lect2-Cre/Rosa26-Tomato* mice were injected with CCl4 to induce fibrosis. Harvested liver tissues were processed for immunofluorescence staining for Alb (hepatocyte marker), CD31 (endothelial marker), α-SMA (activated HSC marker), and F4/80 (macrophage marker). Slides were counterstained with DAPI. Arrows, ECs. Scale bar, 20 μm. C-G, Primary kupffer cells (KC), hepatocytes (PH), endothelial cells (EC) and Hepatic stellate cells (HSC) were isolated from control mice liver or fibrotic mice livers induced by CCl4. (C), western blot assay using anti-LECT2 antibody showed the expression of LECT2. (D), qPCR assay was employed to measure LECT2 mRNA levels in PH, EC, KC and HSC. (E), TGF-β1 induced upregulation of LECT2 mRNA level in PH. (F), TGF-β1 induced upregulation of LECT2 mRNA level in EC. (G), TGF-β1 upregulated LECT2 secretion in PH and EC isolated from WT mice rather than those isolated from *Lect2-KO* mice. Mean ± s.e.m. *p < 0.05, **p < 0.01, ****p < 0.0001.

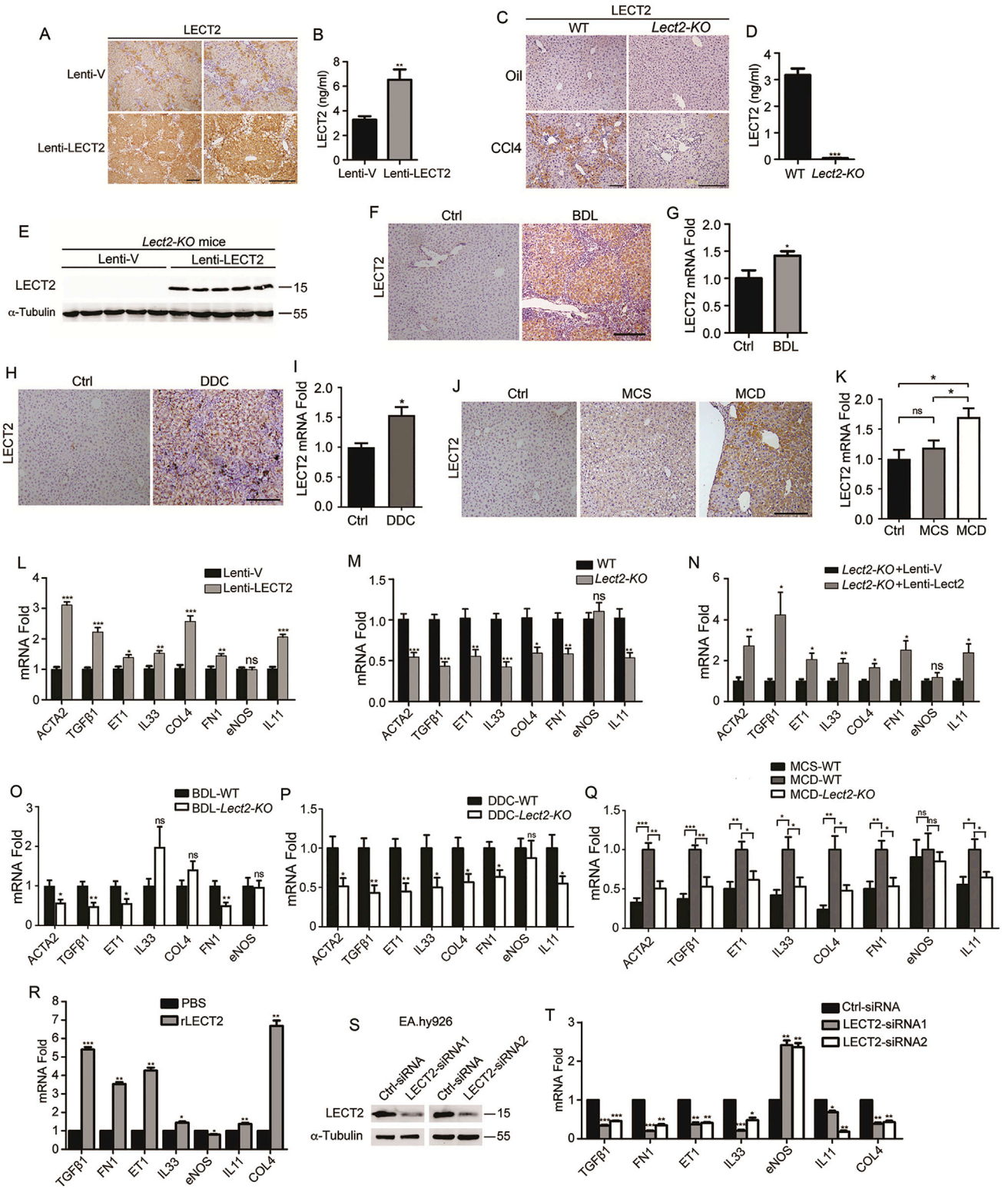

Figure S2. LECT2 Is Upregulated in Multiple Liver Fibrosis Models, Related to Figure 2

A-E, Liver fibrosis models were established in wild-type C57BL/6 mice with LECT2 overexpression by Lenti-LECT2 (A, B), *Lect2-KO* mice (C, D), and *Lect2-KO* mice with LECT2 restoration by Lenti-LECT2 (E) by injecting CCl4 (2 ml/kg in olive oil at a ratio of 1:4, i.p., twice a week for 3 weeks). The mice injected with olive oil alone (Oil) (2 ml/kg, i.p., twice a week for 3 weeks) or infected with the same dose of lentiviral control vector (Lenti-V) were controls. The livers were harvested and

(legend continued on next page)

the LECT2 expression were stained for LECT2 using anti-LECT2 antibody (A, C, E). Scale bar, 200 μm. (B), (D), ELISA assay analyses of the serum level of LECT2. n = 6 mice/group. F, H, (G), Immunohistochemical staining of LECT2 in liver samples from BDL, DDC and MCD-induced liver fibrosis models and their control mice using anti-LECT2 antibody accordingly. Scale bars, 200 μm. G, I, K, qRT-PCR were used to analyze the mRNA level of LECT2 in liver samples from BDL, DDC and MCD models. n = 6 mice/group. L-Q, qRT-PCR were used to analyze the mRNA levels of ACTA2, TGFβ1, ET1, IL33, COL4, FN1, ACTA2, eNOS, and IL11 in livers harvested from Lenti-LECT2 or Lenti-V infected wild-type C57BL/6 mice with CCl4-induced liver fibrosis (L), *Lect2-KO* or control mice with-induced CCl4 liver fibrosis (M), Lenti-LECT2 or Lenti-V infected *Lect2-KO* mice with CCl4-induced liver fibrosis (N), *Lect2-KO* or control mice with BDL-induced liver fibrosis (O), *Lect2-KO* or control mice with DDC-induced liver fibrosis (P), *Lect2-KO* or control mice with MCD-induced liver fibrosis (Q). R, rLECT2 enhanced mRNA levels of TGFβ1, FN1, ET1, IL33, IL11 and COL4, and decreased mRNA levels of eNOS in EA.hy926 cells. (S), LECT2 was knockdown by siRNAs in EA.hy926 cells. (T), LECT2 knockdown decreased mRNA levels of TGFβ1, FN1, ET1, IL33, IL11 and COL4, and enhanced mRNA levels of eNOS in EA.hy926 cells. Mean ± s.e.m. of three independent experiments. n = 6 mice/group. *$p < 0.05$, **$p < 0.01$, ***$p < 0.001$.

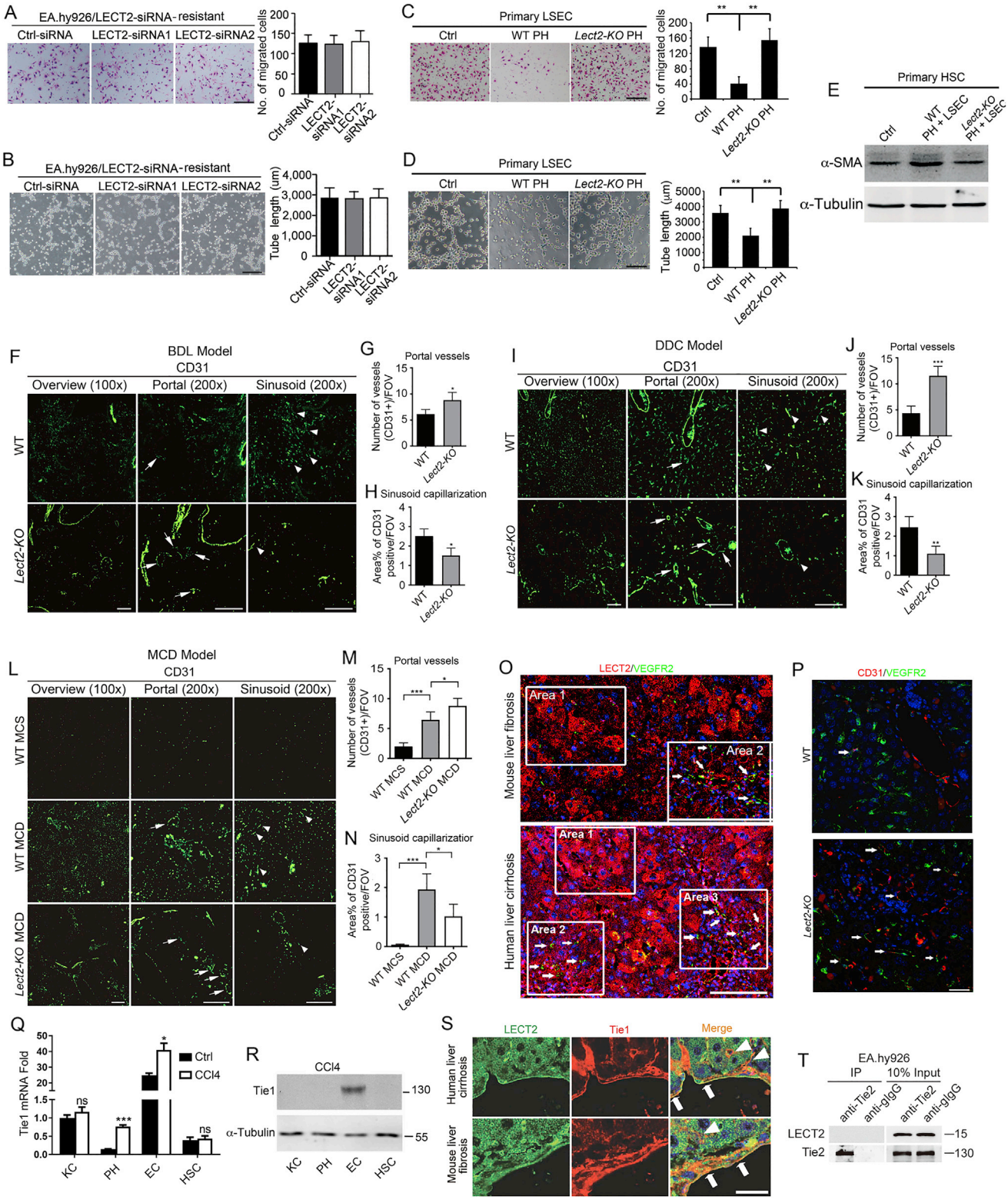

Figure S3. LECT2 Inhibits Angiogenesis and Promotes Capillarization of Liver Sinusoids, Related to Figures 3 and 4

A, B, Plasmids encoding siRNA-resistant LECT2 were transfected into EA.hy926 cells (EA.hy926/LECT2-siRNA-resistant), control siRNA, LECT2 siRNA1 and LECT2 siRNA2 were transfected into EA.hy926/LECT2-siRNA-resistant cells. By transwell assay, LECT2 siRNAs failed to inhibit EA.hy926/LECT2-siRNA-resistant

(legend continued on next page)

cell migration (A). By tube formation assay, LECT2 siRNAs failed to inhibit EA.hy926/LECT2-siRNA-resistant cell tube formation (B). Scale bars, 200 μm. C-E, Primary hepatocytes (PH), liver sinusoid endothelial cells (LSEC) were isolated from wild-type C57BL/6 (WT) mice or *Lect2-KO* mice, primary Hepatic stellate cells (HSC) were isolated from WT mice. LSECs isolated from WT mice were co-cultured with PH isolated from WT mice (WT PH) or *Lect2-KO* mice (*Lect2-KO* PH). (C), By transwell assay, PH from WT mice inhibited LSEC migration, whereas PH from *Lect2-KO* mice could not inhibit LSEC migration. (D), By tube formation assay, PH from WT mice inhibited LSEC tube formation, whereas PH from *Lect2-KO* mice could not. Scale bars, 200 μm. (E), PH isolated from WT mice were co-cultured with LSECs isolated from WT mice (WT PH+LSEC), PH isolated from *Lect2-KO* mice were co-cultured with LSECs isolated from *Lect2-KO* mice (*Lect2-KO* PH+LSEC). The condition medium from WT PH+LSEC co-culture system or from *Lect2-KO* PH+LSEC co-culture system were added into HSCs isolated from WT mice. After 24 hours, HSCs were harvested for α-SMA detection using anti-α-SMA antibody, α-Tubulin was as control. F-H, *Lect2-KO* increased portal angiogenesis, decreased capillarization of liver sinusoids in BDL-induced liver fibrosis models. Scale bars, 200 μm. I-K, *Lect2-KO* increased portal angiogenesis, decreased capillarization of liver sinusoids in DDC-induced liver fibrosis models.Scale bars, 200 μm. L-N, *Lect2-KO* increased portal angiogenesis, decreased capillarization of liver sinusoids in BDL-induced liver fibrosis models. Scale bars, 200 μm. (O), Co-immunofluorescence staining of LECT2 using anti-LECT2 antibody and VEGFR2 using anti-VEGFR2 antibody in mouse liver fibrosis samples (upper) and in human liver cirrhosis samples (lower). DAPI was used to stain the nucleus. Area 1 represents the region with high LECT2 expression, area 2 and area 3 represent the region with low LECT2 expression. Arrow indicates $VEGFR2^{+}$ blood vessels. Scale bar, 50 μm. (P), Co-Immunofluorescence staining of CD31 using anti-CD31 antibody and VEGFR2 using anti-VEGFR2 antibody in livers harvested from WT Control mice or *Lect2-KO* mice with CCl4-induced liver fibrosis. DAPI is used to stain the nucleus. Arrow indicates $CD31^{+}$/$VEGFR2^{+}$ double positive blood vessels. Scale bar, 50 μm. (Q), (R), Primary kupffer cells (KC), hepatocytes (PH), endothelial cells (EC) and Hepatic stellate cells (HSC) were isolated from control mice liver or fibrotic mice liver induced by CCl4. qPCR assay showed that Tie1 was highly expressed in EC (Q). Western blot assay showed that Tie1 was expressed in EC (R). Anti-Tie1 antibody was employed to stain Tie1, α-Tubulin was as control. S, Co-localization of LECT2 and Tie1 in the portal vessels of human and mouse cirrhotic livers. LECT2 and Tie1 were detected using immunofluorescent staining with their respective antibodies. Slides were counterstained with DAPI. Arrows, portal vessels; arrowheads, LSECs. Scale bar: 20 μm. (T), Endogenous LECT2 and Tie2 was immunoprecipitated from the EA.hy926 cell lysates using anti-Tie2 antibodies, followed by immunoblotting for LECT2 (~17 kDa) and Tie2 (~130 kDa). LECT2 did not interact with Tie2. Mean, ± s.e.m. $^{*}p < 0.05$, $^{**}p < 0.01$, $^{***}p < 0.001$.

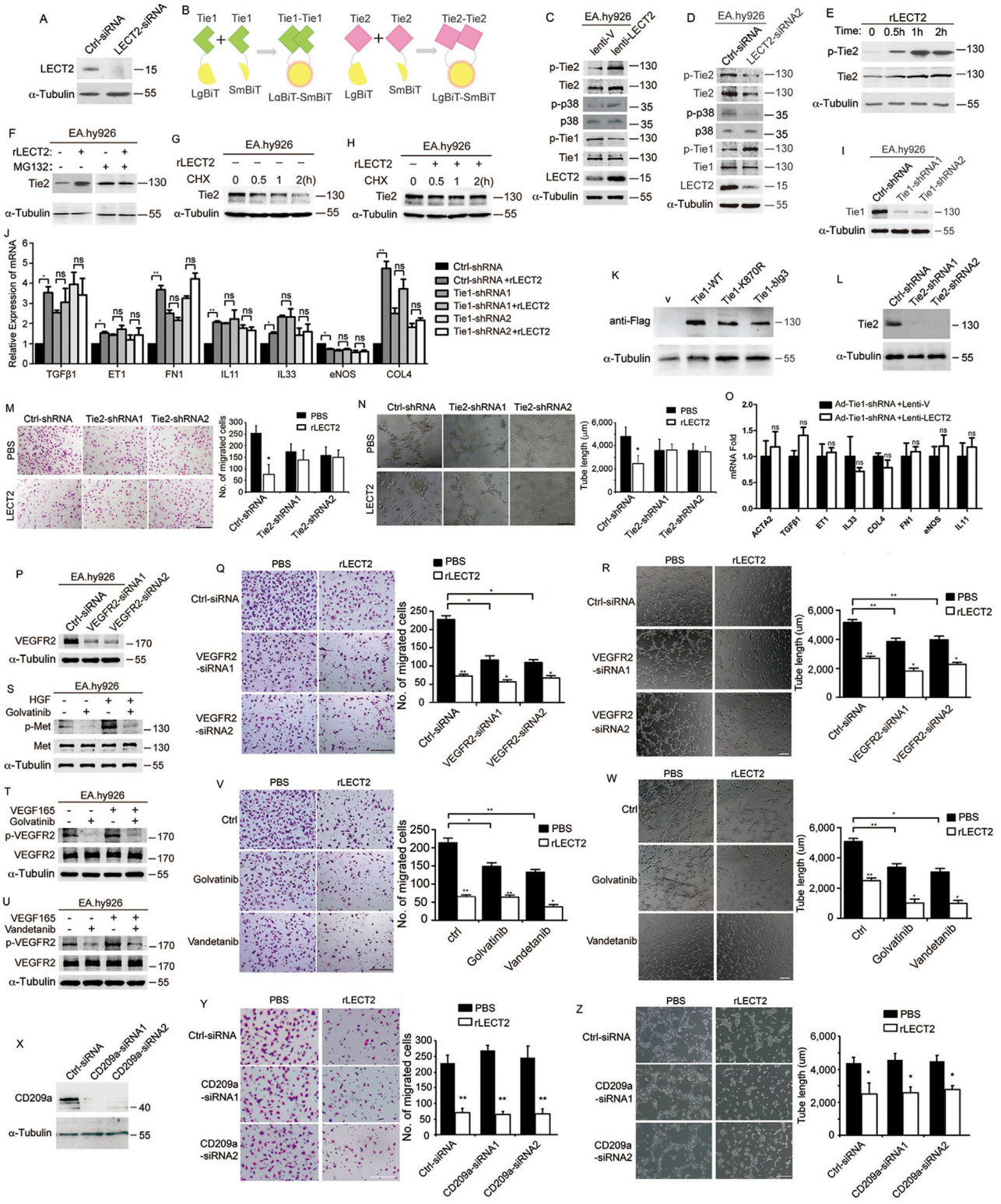

Figure S4. Tie1 Is Required for LECT2 to Exert Functional Impacts on ECs, Related to Figure 5

(A), LECT2-siRNA was used to knock down LECT2 in 293T cells. (B), Schematic illustration of NanoBiT Protein:Protein interactions system for Figure 5D. Large BiT (LgBiT; 17.6kDa) and Small BiT (SmBiT; 11 amino acids) subunits were fused to Tie1 or Tie2, for Tie1/Tie1 interactions and Tie2/Tie2 interactions. Tie1/LgBiT together with Tie1/SmBiT were transfected into LECT2 knock-down 293T cells for Tie1-Tie1 interaction measurement, Tie2/LgBiT together with Tie2/SmBiT were

(legend continued on next page)

transfected into LECT2 knock-down 293T cells for Tie2-Tie2 interaction measurement. (C), Lenti-LECT2 increased Tie2 phosphorylation and total Tie2 levels, increased p38 phosphorylation, and reduced Tie1 phosphorylation in EA.hy926 cells. (D), Knockdown of LECT2 using siRNA reduced Tie2 phosphorylation and total Tie2 levels, reduced p38 phosphorylation, and increased Tie1 phosphorylation in EA.hy926 cells. E, Phosphorylation of Tie2 induced by LECT2 was time-dependent. F, EA.hy926 cells were treated with MG132 (5 μM), in the absence or presence of rLECT2, for 6 hours. Cell lysates were immunoblotted with antibodies to Tie2 and α-Tubulin. G, H, EA.hy926 cells were treated with CHX, in the absence or presence of rLECT2, for a period of time as indicated. Cell lysates were immunoblotted with antibodies to Tie2 and α-Tubulin. I, Tie1-shRNA1 and Tie1-shRNA2 downregulated Tie1 in EA.hy926 cells. (J), qRT-PCR were used to analyze the mRNA levels of TGFβ1, FN1, ET1, IL33, ACTA2, COL4, AC7A2, eNOS and IL11 in EA.hy926 cells transfected with control siRNA, Tie1-siRNA1 or Tie1-siRNA2. (K), Wild-type Tie1 (Tie1-WT), kinase dead Tie1 (Tie1K870R) and Ig3 deletion Tie1 (Tie1-δIg3) were transfected into EA.hy926 cells, their expressions were detected by immunoblotting using anti-Flag antibody. α-Tubulin was as control. L, Tie2-shRNA1 and Tie2-shRNA2 downregulated Tie2 in EA.hy926 cells. (M), By transwell assay, rLECT2 failed to inhibited EA.hy926 cell migration when Tie2 was knocked down. (N), By tube formation assay, rLECT2 failed to inhibited EA.hy926 cell tube formation when Tie2 was knocked down. (O), Six-week-old male wild-type C57 mice infected with Ad-Tie1-shRNA and Lenti-LECT2 or Lenti-V, were injected with CCl4 (2 ml/kg, in olive oil at a ratio of 1:4, i.p., twice a week for 3 weeks). Hepatic mRNA levels of ACTA2, TGFβ1, ET1, IL33, COL4, FN1, eNOS, and IL11 were measured by qRT-PCR. (P), VEGFR2 was knocked down by siRNAs in EA.926 cells. (Q), By transwell assay, rLECT2 inhibited EA.hy926 cell migration when VEGFR2 was knocked down. (R), By tube formation assay, rLECT2 inhibited EA.hy926 cell tube formation when VEGFR2 was knocked down. (S), (T), Phosphorylation of VEGFR2 was inhibited by its inhibitor Golvatinib. (U), Phosphorylation of Met and VEGFR2 were inhibited by their inhibitor Vandetanib. (V), By transwell assay, rLECT2 inhibited EA.hy926 cell migration when MET or/and VEGFR2 was inhibited by Golvatiniband Vandetanib. (W), By tube formation assay, rLECT2 inhibited EA.hy926 cell tube formation when MET or/and VEGFR2 was inhibited by Golvatiniband Vandetanib. (X), CD209a was knockdown by siRNAs in EA.926 cells. (Y), By transwell assay, rLECT2 inhibited EA.hy926 cell migration when CD209a was knocked down. (Z), By Tube formation assay, rLECT2 inhibited EA.hy926 cell tube formation when CD209a was knocked down. Scale bar, 200 μm. Mean ± s.e.m. *$p < 0.05$, **$p < 0.01$.

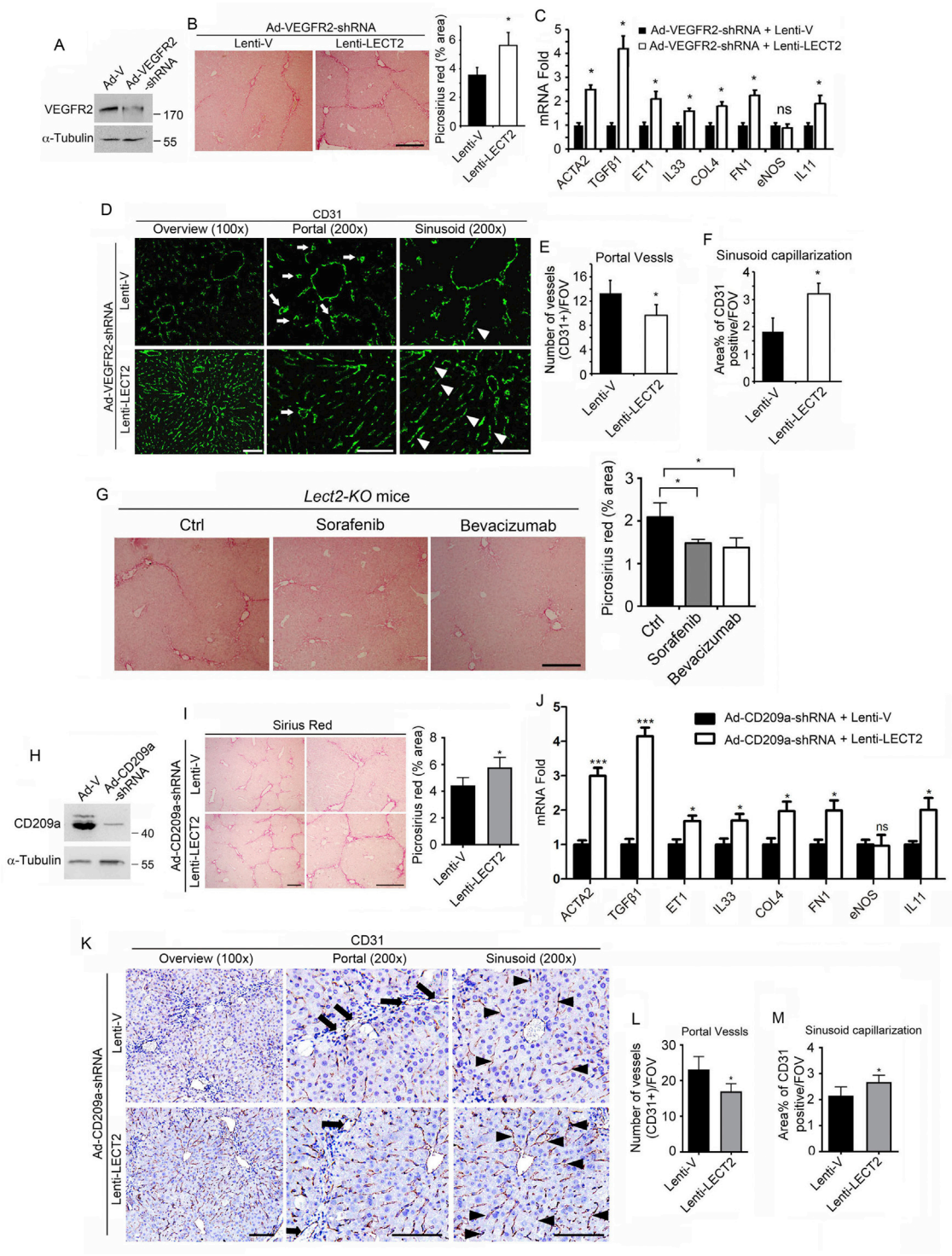

Figure S5. Tie1 Is Required for LECT2 to Promote Liver Fibrogenesis, Related to Figure 5

A-F, Six-week-old male wild-type C57 mice infected with Ad-VEGFR2-shRNA, and Lenti-LECT2 or Lenti-V, were injected with CCl4 (2 ml/kg, in olive oil at a ratio of 1:4, i.p., twice a week for 3 weeks). The livers were processed for western blot (A) and Sirius Red staining (B). Hepatic mRNA levels of ACTA2, TGFβ1, ET1, IL33, COL4, FN1, eNOS, and IL11 were measured by qRT-PCR (C). Immunohistochemical staining for CD31 (D), and the numbers of CD31+ vessels surrounding portal area (E) and the CD31+ capillarization of liver sinusoids (F) were measured. Scale bar, 200 μm. (G), Six-week-old wild-type *Lect2-KO* mice were i.p. injected with CCl4 (2 ml/kg, Sigma-Aldrich) dissolved in olive oil at a ratio of 1:4, twice a week for 3 weeks. VEGF-VEGFR inhibitor sorafenib and bevacizumab were injected into mice through tail vein at the beginning of CCl4 treatment. After 3 weeks, the livers were harvested and stained using Sirius Red for fibrosis analysis. Scale bar,

(legend continued on next page)

200 μm. n = 6 mice/group. H-M, Six-week-old male wild-type C57 mice infected with Ad-CD209a-shRNA, and Lenti-LECT2 or Lenti-V, were injected with CCl4 (2 ml/kg, in olive oil at a ratio of 1:4, i.p., twice a week for 3 weeks). The livers were processed for western blot (H) and Sirius Red staining (I). Hepatic mRNA levels of ACTA2, TGFβ1, ET1, IL33, COL4, FN1, eNOS, and IL11 were measured by qRT-PCR (J). Immunohistochemical staining for CD31 (K), and the numbers of CD31+ vessels surrounding portal area (L) and the CD31+ capillarization of liver sinusoids (M) were measured. Scale bar, 200 μm. n = 6 mice/group. *$p < 0.05$, **$p < 0.01$, ***$p < 0.001$.

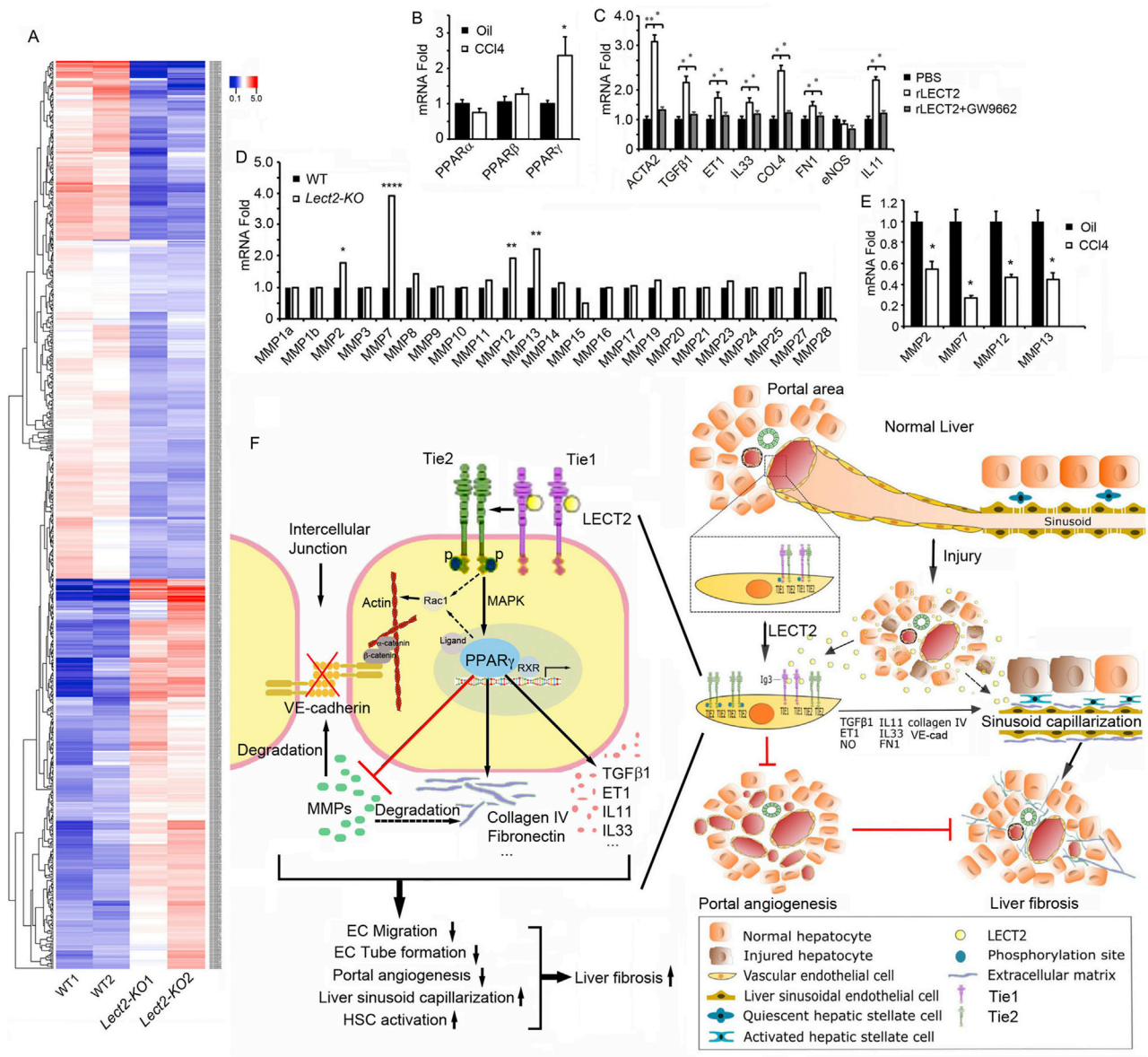

Figure S6. LECT2-Tie1 Signaling Pathway, Related to Figure 6

A, RNaseq was used to analyze the differential gene expression between wild-type and *Lect2-KO* mice in a CCl4-induced fibrosis model. Six-week-old male wild-type C57BL/6 mice were injected with CCl4 (2 ml/kg, in olive oil at a ratio of 1:4, i.p., twice a week for 3 weeks). The livers were harvested for RNaseq analysis. Heatmap showed 689 genes differentially expressed in liver tissues (with a p value < 0.05 and a Fold Change > 2). B, Liver tissues from control (Oil) or CCl4 treated wild-type mice were harvested for measuring the expression of PPARs, using qPCR assay. (C), PPARγ inhibitor GW9662 reversed the effects of rLECT2 on the expression of fibrotic factors in EA.hy926 cells. qRT-PCR assay was used to analyze the mRNA levels of TGFβ1, FN1, ET1, IL33, ACTA2, COL4, AC7A2, eNOS and IL11 in EA.hy926 cells treated with rLECT2 alone or rLECT2 plus GW9662. (D), The mRNA level of MMPs in WT and *Lect2-KO* mice according to RNaseq data. MMP2, MMP7, MMP12 and MMP13 were upregulated in *Lect2-KO* mice compared to wild-type control mice. (E), Liver tissues from control (Oil) or CCl4 treated wild-type mice were harvested for measuring the expression of MMPs, using qPCR assay. (F), Schematic illustration of our proposed model. Upon injury, increased LECT2 is secreted by hepatocytes around portal area and damage boundaries. LECT2 binds directly to Ig3 domain of EC receptor Tie1, interrupts Tie1/Tie2 interactions, phosphorylates Tie2 and MAPK, activates PPARγ, inhibits the expression of MMPs and induces the expression of fibrotic factors. Downregulation of MMPs results in accumulations of extracellular matrix and VE-cadherin. Increased VE-cadherin enhances EC-EC intercellular junction, inhibits EC migration and tube formation, inhibits portal angiogenesis. Both extracellular matrix accumulation and EC-EC intercellular junction enhancement facilitate liver sinusoid capillarization. Fibrotic factors and liver sinusoid capillarization activate HSC. All of these events lead to liver fibrogenesis. Mean ± s.e.m. *p < 0.05. **p < 0.01.

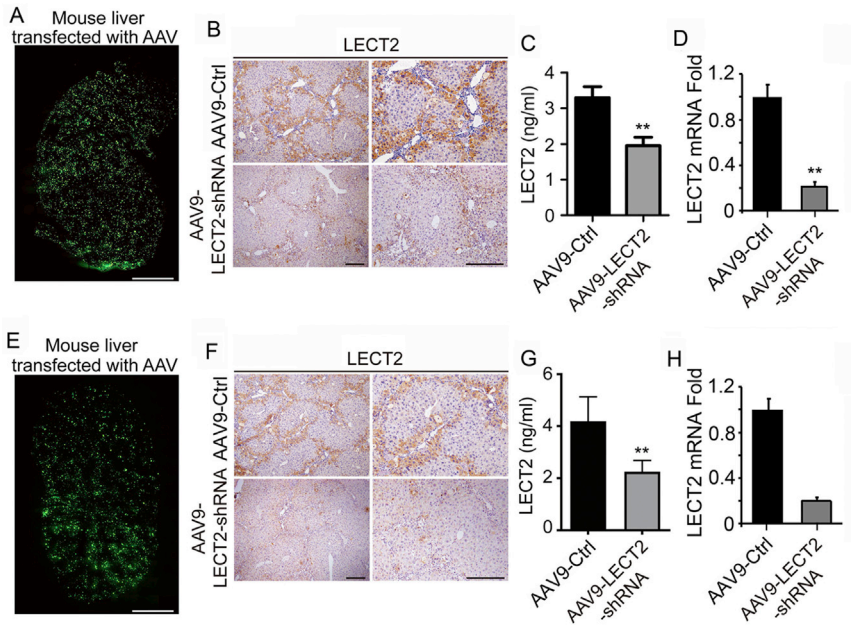

Figure S7. AAV9-LECT2-shRNA Infection, Related to Figure 7

A-D, Six-week-old male wild-type C57BL/6 mice were i.p. injected with CCl4 (2 ml/kg, Sigma-Aldrich) dissolved in olive oil at a ratio of 1:4, or olive oil alone (2 ml/kg) twice a week for 3 weeks. AAV9 control vector (AAV9-Ctrl) or AAV9-LECT2-shRNA were injected into mice through tail vein. (A), Overall view of mouse liver infected with AAV9. Scale bar, 2.5mm. (B), AAV9-LECT2-shRNA reduced LECT2 level in liver. Immunohistochemical staining of LECT2 using anti-LECT2 antibody in liver tissue sections harvested from AAV9-Ctrl or AAV9-LECT2-shRNA infected mice. Scale bars, 100 μm. (C), AAV9-LECT2-shRNA reduced serum LECT2 level in AAV9-LECT2-shRNA infected mice, as compared to those in AAV9-Ctrl infected mice. The serum LECT2 level was measured using ELISA kit. D, qPCR analysis showed AAV9-LECT2-shRNA reduced mRNA level of LECT2 in AAV9-LECT2-shRNA infected mice, as compared to those in AAV9-Ctrl infected mice. E-H, Six-week-old wild-type male C57BL/6 mice were i.p. injected with CCl4 (2 ml/kg, Sigma-Aldrich) dissolved in olive oil at a ratio of 1:4, twice a week for 3 weeks. AAV9 control vector (AAV9-Ctrl) or AAV9-LECT2-shRNA were injected into mice through tail vein 3 weeks after CCl4 treatment. After another 3 weeks, the livers and serum were harvested for analysis. (E), Overall view of mouse liver infected with AAV9. Scale bar, 2.5mm. (F), AAV9-LECT2-shRNA reduced LECT2 level in liver. Immunohistochemical staining of LECT2 using anti-LECT2 antibody in liver tissue sections harvested from AAV9-Ctrl or AAV9-LECT2-shRNA infected mice. Scale bars, 100 μm. (G), AAV9-LECT2-shRNA reduced serum LECT2 level in AAV9-LECT2-shRNA infected mice, as compared to those in AAV9-Ctrl infected mice. The serum LECT2 level was measured using ELISA kit. H, qPCR analysis showed AAV9-LECT2-shRNA reduced mRNA level of LECT2 in AAV9-LECT2-shRNA infected mice, as compared to those in AAV9-Ctrl infected mice. n = 6 mice/group. Mean ± s.e.m. **p < 0.01.